Programmed Variations of Cytokinesis Contribute to Morphogenesis in the *C. elegans* embryo

Xiaofei Bai[1], Po-Yi Lee[3], Chin-Yi Chen[3], James R. Simmons[1], Benjamin Nebenfuehr[1,4], Diana Mitchell[1,5], Lindsey R. Klebanow[1,6], Nicholas Mattson[1,7], Christopher G. Sorensen Turpin[1], Bi-Chang Chen[2,3], Eric Betzig[2], Joshua N. Bembenek[1*]

[1] Department of Biochemistry, Cellular and Molecular Biology, University of Tennessee, Knoxville, Tennessee, United States of America.
[2]Janelia Research Campus, HHMI, Ashburn, Virginia, United States of America.
[3]Research Center for Applied Science, Academia Sinica, Taiwan.
[4]Current Address: NIDDK, NIH, Bethesda, MD, United States of America.
[5]Current Address: Biological Sciences, University of Idaho, Moscow, Idaho, United States of America.
[6]Current Address: Parker Hannefin Corporation, Macedonia, Ohio, United States of America
[7]Current Address: USFDA/CDER/OPQ/OBP/DBRRI, Silver Springs, MD, United States of America

* Corresponding Author:
Joshua N. Bembenek
1414 Cumberland Ave.
C211 Walters Life Sciences Building
Knoxville, TN 37996
(865)-974-4085
E-mail: bembenek@utk.edu

Abstract

While cytokinesis has been intensely studied, how it is executed during development is not well understood, despite a long-standing appreciation that various aspects of cytokinesis vary across cell and tissue types. To address this, we investigated cytokinesis during the invariant lineage of the *C. elegans* embryo and find that several parameters are reproducibly altered in different stages. During early divisions, cells undergo consistent patterns of furrow ingression asymmetry and midbody inheritance, suggesting specific regulation of these events. During morphogenesis, in the intestine, pharynx, and amphid sensilla, we find several alterations including migration of midbodies to the apical surface during cellular polarization. In each tissue, Aurora B kinase localizes to the apical membrane after internalization of other midbody components. Perturbations of cytokinesis disrupt lumen formation and dendrite formation. Therefore, cytokinesis shows surprising diversity during development, and may regulate the final interphase architecture of a terminally dividing cell during morphogenesis.

Introduction

Generation of a multicellular organism requires that carefully orchestrated cell division is integrated properly into different developmental processes. Cell division is required not only to generate new cells that organize into tissues, but also to dictate the size, position and timing of daughter cells that are generated. Several aspects of cell division, including spindle orientation and division symmetry are well known instruments of developmental programs (Siller and Doe, 2009). Roles for cytokinesis in regulating developmental events are emerging, but are much less understood (Chen et al., 2013; Herszterg et al., 2014; Li, 2007). Using advanced live imaging, we sought to investigate cytokinesis in the well-defined divisions of the invariant *C. elegans* embryo lineage, which has been completely described (Sulston et al., 1983).

Cytokinesis is the final step of cell division and is normally a constitutive process during the exit from mitosis defined by discrete steps that occur during "C phase" (Canman et al., 2000; Oegema and Hyman, 2006). During cell division, signals from the anaphase spindle initiate ingression of the cleavage furrow (Bringmann and Hyman, 2005; Eggert et al., 2006), which constricts the plasma membrane onto the spindle midzone and leads to formation of the midbody. The midbody is a membrane channel between daughter cells containing microtubules and a defined organization of more than one hundred proteins that collaborate to execute abscission, the final separation of daughter cells (Green et al., 2012; Hu et al., 2012; Skop et al., 2004). Many of the proteins that contribute to midbody formation and function have roles in the formation of the central spindle and the contractile ring (El Amine et al., 2013). In addition, vesicles are delivered to the midbody that contribute lipids as well as regulators of abscission (Schiel et al., 2013). Subsequently, the ESCRT machinery assembles, microtubules are cleared and membrane scission occurs (Guizetti et al., 2011; Schiel et al., 2011). Aurora B kinase (AIR-2 in *C. elegans*) is required for the completion of cytokinesis, and also regulates the timing of abscission in response to developmental or cell cycle cues partly by regulating the ESCRT machinery (Carlton et al., 2012; Carmena et al., 2015; Mathieu et al., 2013; Norden et al., 2006; Steigemann et al., 2009). Substantial effort has been devoted to understanding factors required to assemble the midbody and the mechanisms of regulation and execution of abscission. In general, while mechanistic details are being elucidated, it is generally assumed that these events occur through a standard, well-defined series of ordered events.

Exceptions to such a clear linear view of cytokinetic events have long been known, but are considered to be specialized cases. The most extreme examples are cells that do not complete cytokinesis altogether and become polyploid, such as liver or intestinal cells (Amini et al., 2015; Fox and Duronio, 2013; Hedgecock and White, 1985; Lacroix and Maddox, 2012). Another well-known example is found in several systems where germ cells do not complete abscission and remain connected through ring canals, which can allow flow of cytoplasm into germ cells (Greenbaum et al., 2007; Haglund et al., 2011; Hime et al., 1996; Maddox et al., 2005). Delayed abscission has also been observed in other cell types to keep daughter cells connected (McLean and Cooley, 2013; Zenker et al., 2017). Other variations of cytokinesis include cleavage furrow re-positioning during anaphase to change the size and fate of daughter cells (Ou et al., 2010). The symmetry of furrow ingression is important in established epithelial tissue where the furrow constricts toward the apical side of the cell and must occur while appropriate cellular contacts are preserved (Herszterg et al., 2014). In zebrafish neuroepithelial divisions, asymmetrical furrowing positions the midbody at the apical domain, which is inherited by the differentiating daughter (Paolini et al., 2015). Therefore, there are a number of ways the standard pattern of cytokinesis can be altered and more investigation is required to understand the functional purpose of these changes and how they are achieved.

Recent studies of abscission have sparked renewed interest in the midbody, which has led to insights into other functions it has beyond abscission (Chen et al., 2013). In general, the midbody is cut off from each of the daughter cells that give rise to it (Crowell et al., 2014; Konig et al., 2017). The midbody may then be engulfed by either cell or persist extracellularly, which can depend on cell type (Ettinger et al., 2011; Salzmann et al., 2014). The midbody can also travel to non-parent cells, suggesting that it may carry or transport signals between cells (Crowell et al., 2014). The midbody is reproducibly inherited in *Drosophila* germline stem cells, but does not always end up in the stem cell (Salzmann et al., 2014). In dividing neuroepithelial cells, a stem cell marker is concentrated at the midbody and released into the lumen of the neural tube, which might provide signals during neuronal development (Dubreuil et al., 2007). This has led to the hypothesis that the midbody provides cues that regulate cell fate, although a detailed mechanistic understanding of this has not been elucidated.

A more clearly defined function for the midbody has been uncovered in cells that undergo polarization events after the completion of cytokinesis. For example, Madin-Darby canine kidney (MDCK) cells can establish apical basal polarity and organize into a simple epithelial lumen structure (Reinsch and Karsenti, 1994). Apical membrane markers are first delivered to the midbody during cytokinesis, establishing an apical membrane at the interface between the first two daughter cells (Schluter et al., 2009). Proper abscission and midbody positioning is required, in addition to proper spindle orientation, for MDCK lumen formation (Lujan et al., 2016; Reinsch and Karsenti, 1994). Polarized trafficking during cytokinesis has been shown to promote lumen formation in other systems as well (Wang et al., 2014b). Abscission is also delayed in acentrosomal blastomeres of the early mouse embryo to generate a midzone-derived microtubule organizing center that directs delivery of apical membrane markers to the plasma membrane (Zenker et al., 2017). The midbody becomes the apical process in chick neuronal progenitors (Wilcock et al., 2007) and defines the site of polarization for dendrite extension in *D. melanogaster* neurons (Pollarolo et al., 2011). The midbody is also a polarizing cue in the *C. elegans* embryo during the establishment of dorsoventral axis formation (Singh and Pohl, 2014; Waddle et al., 1994). In addition, the midbody can play a role in cilium formation (Bernabe-Rubio et al., 2016). Further effort is required to understand how cytokinesis and the midbody regulate pattern formation in tissues.

In order to further investigate patterns of cytokinesis during development, we examined the invariant *C. elegans* lineage. We find that cytokinesis follows a lineage specific pattern and that furrow symmetry and midbody inheritance is highly reproducible. During morphogenesis, we observe striking midbody migration events in the developing digestive and sensory tissues in *C. elegans*, likely before abscission. Interestingly, AIR-2 migrates with midbodies and remains at several apical surfaces after internalization of different ring components. Coordinated movements of midbodies and differential fates of midbody components are novel behaviors during cytokinesis and are programmed at specific divisions in the embryo. Inactivation of temperature-sensitive midbody proteins disrupt proper formation of several tissues, indicating an important role for specialized cytokinesis during morphogenesis. Together, our results reveal that coordinated alterations in cytokinesis regulation, particularly with regards to the midbody, are critical for proper animal development.

Results

Cytokinesis in the first two mitotic divisions: asymmetric midbody inheritance

We sought to systematically examine cytokinesis using lattice light sheet and spinning disc confocal microscopy during the stereotypical divisions of the *C. elegans* embryo, which has been extensively studied primarily in the first cell division due to its size and ease of access. The first division of the P0 cell generates the larger anterior daughter AB and the posterior daughter P1 (Fig. 1 A). We observed different components that allow us to evaluate specific aspects of the cytokinetic apparatus including the central spindle, the cytokinetic furrow and the midbody. We also chose midbody markers that localize to the flank and ring sub-structures of the midbody (Green et al., 2012). To observe the midbody flank region, we imaged the Aurora B kinase, AIR-2, microtubules, and the membrane trafficking regulator RAB-11 (Fig. 1, 3, and Video S1). We also imaged midbody ring markers including the non-muscle myosin NMY-2 and the centralspindlin component ZEN-4 (Fig. 1 G-P and Video S1). While the first mitotic furrow shows some variable asymmetry as previously demonstrated (Maddox et al., 2007), the midbody forms in a relatively central position between daughter cells (Fig. 1 B-C, G-H and L-M). AIR-2::GFP, endogenous AIR-2 staining and tubulin show the expected pattern of localization on the central spindle and midbody as expected (Fig. 1 B-C, Fig. S1 A-D, Fig. 3 A-B and Video S1). The midbody from the first mitotic division is always inherited by the P1 daughter cell (Fig. 1 A) (Bembenek et al., 2013; Singh and Pohl, 2014). The midbody microtubule signal diminishes within 8 minutes after furrowing onset, which is a general indicator of abscission timing (Fig. 3 B, I) (Green et al., 2013; Konig et al., 2017). AIR-2 is lost from the flank over time but can be observed on the midbody remnant even after it is internalized into P1 (Fig. 1 D-E and Video S1). Additionally, each of the ring components behaves similarly to AIR-2, as expected (Fig. 1 I-J and N-O). Therefore, AIR-2 and other ring components remain co-localized on the midbody throughout the final stages of cytokinesis and are reproducibly internalized by the P1 daughter cell, as previously observed (Bembenek et al., 2013; Ou et al., 2014; Singh and Pohl, 2014).

During the second round of division, we observed substantial, reproducible changes in the pattern of cytokinesis, beginning with furrow symmetry. During the AB daughter cell division, which gives rise to ABa and ABp, the furrow ingressed

from the outer surface until it reached the opposite plasma membrane in contact with EMS (Fig. 1 D-E, I-J, N-O). We calculated a symmetry parameter using the ratio of furrow ingression distance from each side of the furrow at completion (Maddox et al., 2007). On average, the furrow symmetry parameter is 1.7 in the first division, while the AB furrow is 21.6 and the P1 furrow is 16.1, indicating highly asymmetric furrows in the second divisions (Fig. 1 V, X). The central spindle is swept from the middle of the AB cell into contact with EMS during furrow ingression (Fig. 1 E, Video S1). AIR-2 localizes to the central spindle, then the midbody flank and remains associated with the midbody remnant after it is engulfed (Fig. 1 D-F, S-U and Video S1). NMY-2 and ZEN-4 also follow the expected pattern during cytokinesis and appear on the midbody that forms in contact with EMS (Fig. 1 I-J, N-O and Video S1). RAB-11::GFP in both the first and second rounds of division accumulates briefly prior to abscission and is not observed on the midbody afterward (Figure 1 Q-U), as shown previously (Ai et al., 2009; Bai and Bembenek, 2017; Bembenek et al., 2010). Therefore, all midbody markers examined behave as expected, localizing to the midbody, which is internalized after abscission is completed.

Our examinations of the midbody confirmed the unexpected and consistent pattern of inheritance during the AB division. The midbody from the AB cell division that forms in contact with EMS after highly asymmetric furrowing is invariably engulfed by EMS instead of either of the AB daughter cells (Fig. 1 F, K, P, U, Fig S1 D and Video S1). Further, the midbody from the P0 division is also always inherited by EMS. Microtubules in the midbody flank disappear within 8 minutes after furrowing in both AB and P1 cell divisions, indicative of relatively fast abscission at this stage (Fig. 3 C-D and I). Therefore, a consistent pattern of cytokinesis is observed during the first two divisions, involving reproducible furrow ingression symmetry and midbody inheritance. Multiple mechanisms operating during cytokinesis must be properly regulated in order to achieve this highly reproducible pattern. This analysis confirms expected patterns of midbody regulation and midbody protein dynamics during the early embryonic divisions and indicates careful regulation of cytokinesis.

Cytokinesis in the intestine epithelia: midbody migration to the apical surface

We next performed a similar analysis of cytokinesis on three developing tissues during morphogenesis, which revealed novel cytokinesis patterns in each. During embryonic morphogenesis, cells undergo terminal divisions and start to form tissues

by polarizing and changing shape. The intestine is a well-studied epithelial tube derived from the E blastomere that undergoes five well defined divisions (Leung et al., 1999). The E8 to E16 division occurs around 280 minutes after the first cleavage, after which cells undergo a mesenchyme to epethelial transition involving epithelial polarization and subsequently organize into a tube (Leung et al., 1999). Our observations demonstrate that these cells are performing cytokinesis as they undergo polarization, which to our knowledge has not been previously reported (Fig. 2 A). The E8 cells undergo relatively symmetrical furrowing that produces a centrally placed midbody (Fig. 2 B, E, I, Fig. S2 A and Video S2-4) with a 1.0 symmetry parameter (Fig 1 W, X), in contrast with the highly asymmetric furrow and displaced midbody location during the AB cell division. Therefore, the E8-E16 division appears largely routine up until the point of midbody formation.

After midbody formation, there are several changes to the pattern of cytokinesis, which occur as the cells polarize. Using lattice light sheet imaging, we observe that centrally located midbodies from both left and right daughter cell divisions (Ealp, Earp, Epla and Epra) migrate across the width of the cell to the nascent apical surface at the midline, which completes 30 minutes after furrow ingression (Fig. 2 B-D and Video S2). The midbody flank region elongates during the migration process and the flank microtubules persist for over 25 minutes on average from furrow ingression to when they join other microtubules at the apical midline and can no longer be distinguished, which is three times longer than the early divisions (Fig. 3 F, H-I). AIR-2::GFP localizes along the extended length of the flank microtubules that move to the apical midline instead of becoming confined to the midbody remnant as observed in early divisions (Fig. 2 E-H, M, and Video S2-4). The ratio of the length of this midbody flank relative to the cell at the greatest length is 0.47 (average 4.6 μm / 9.8 μm) in the intestinal cell division, which is more than twice that of the early two cell divisions 0.17 (average 9.3 μm/ 53.4 μm) in P0 and 0.17 (average 7.7 μm/ 44.3 μm) in AB (Fig. 2 P-Q). The ring markers ZEN-4 and NMY-2 are quickly internalized (553±140 seconds and 545±179 seconds, respectively) after the midbody reaches the apical midline (Fig. 2 I-L, N-O and Video S3). Collectively, these data indicate that abscission occurs after migration of the midbody to the apical midline. Therefore, E8 cells undergo a novel programmed apical midbody migration event instead of having an asymmetrical furrow lead to the formation of an apically

localized midbody, as observed in the AB cell division and epithelial cells in other systems.

Next, we noticed that not all midbody components are internalized the end of cytokinesis and some remain on the apical surface. In contrast to the midbody ring components, AIR-2 persists at the apical midline well after the time that ring components are internalized and polarization is complete (Fig. 2 D, G, H, M and Video S2-4), co-localizing with the apical polarity marker PAR-6 (Fig S2 F-H). Endogenous AIR-2 can also be observed at the apical midline by immunofluorescence (Fig. S1 E-G). The gut apical surface recruits pericentriolar material donated by the centrosome during E16 polarization (Feldman and Priess, 2012; Yang and Feldman, 2015). We observed that γ-tubulin::GFP moves to the apical surface at the same time as AIR-2::GFP (Fig. S2 I). High temporal resolution single plane confocal imaging to track individual midbody dynamics confirm the elongated AIR-2::GFP flank localization and persistence at the apical midline as well as the rapid internalization of ZEN-4::GFP after the migration event (Fig. 2 M-N and Video S4). Therefore, different midbody components have different fates after cytokinesis in the E8-E16 intestinal divisions, with ring markers being internalized while AIR-2 remains at the apical surface. To our knowledge, this is the first report of AIR-2 localization remaining at the plasma membrane after abscission, in most cases it remains on the midbody remnant that is internalized as observed in the early embryo as described above.

In other lumen forming systems, such as MDCK cells, RAB-11 vesicle trafficking during cytokinesis transports apical membrane components to the midbody to establish the apical membrane (Schluter et al., 2009). In *C. elegans*, RAB-11 endosomes control trafficking at the apical surface of the intestine throughout the life of the animal (Sato et al., 2014). We imaged RAB-11 during the E8-E16 division to examine when apical localization occurs. RAB-11::mCherry colocalizes with AIR-2::GFP once the midbody is formed and migrates to the apical surface with the midbody (Fig. S2 J-L). RAB-11::mCherry is also localized at spindle poles, as in other mitotic cells (Albertson et al., 2005), which also migrate to the apical surface (Feldman and Priess, 2012). Similar to AIR-2, RAB-11 remains localized to the apical surface and appears to remain at this position throughout the life of the animal (Fig. S2 L). These observations indicate that the apical localization of RAB-11 is established during cytokinesis in the E8-E16 division and is delivered at least in part

by both the midbody and centrosome. Therefore, cytokinesis is programmed to occur in a specialized way during the E8-E16 division, which may contribute to formation of the apical surface during intestinal epithelial polarization.

The anterior and posterior pair of E16 cells (Ealaa, Earaa, Eplpp and Eprpp) undergo one last division to achieve the E20 intestine stage. In the four central E8 cells that do not divide again, the midbody migrates to the midline at E8-E16 as described above. However, the midbodies from the other four E8 cells (Eala, Eara, Eplp and Eprp), which undergo another division, migrate toward the midline but the AIR-2 signal diminishes (Fig. S2 E). During the terminal E16-E20 divisions, the midbodies of Ealaa, Earaa, Eplpp and Eprpp undergo apical migration after symmetrical furrowing (Fig. S2 M-O and Video S5). Therefore, the midbody migration event in the intestine does not happen only during the polarization event that occurs during E8-E16, suggesting that it is specifically programmed to occur during the terminal embryonic divisions. Post-embryonic divisions in the intestine at L1 lethargus involve nuclear but not cytoplasmic divisions leading to the formation of binucleate cells that subsequently undergo multiple rounds of endoreduplication to become highly polyploid (Hedgecock and White, 1985). Therefore, cytokinesis in the intestinal lineage undergoes distinct regulatory phases at different stages of development.

Gut lumen formation is disrupted in cytokinesis mutants

Given the pattern of cytokinesis during the E8-E16 division and the localization of AIR-2::GFP to apical structures, we sought to investigate whether cytokinesis is important for lumen formation. First, we assessed whether cytokinesis is essential for embryo viability during later development since it is possible that embryos could still hatch even if terminal divisions fail and morphogenesis occurs with multinucleated cells. To bypass the essential function of cytokinetic regulators during the early embryonic cell divisions, we inactivated temperature sensitive (ts) mutants after isolation of two-cell embryos at the permissive temperature (15 °C) and shifted them to non-permissive temperature (26 °C) at different embryo stages until they hatched. The *air-2 (or207ts)* embryos have only 53.6% (37/69) hatching even when left at 15 °C through hatching, indicating that this mutant is sick even at permissive temperature, while wild-type N2, *zen-4 (or153ts)* and *spd-1 (oj5ts)* embryos are 100% viable when kept at 15 °C (Table 1). Embryos shifted to 26 °C after 4.5 hours at 15 °C

(corresponding to late E4 to early E8 stages) showed significantly increased lethality in both *air-2(or207ts)* and *zen-4 (or153ts)*, but not *spd-1 (oj5ts)* (Table 1), which correlates with the amount of cytokinesis failure observed. The few animals that were able to hatch in *air-2(or207ts)* and *zen-4 (or153ts)* mutants had severe morphogenesis defects (data not shown). Mutant embryos shifted after the completion of all the developmental divisions at the comma to 1.5-fold stage were largely rescued for lethality and hatched at a rate similar to permissive temperature (Table 1). Therefore, these results are consistent with the hypothesis that cytokinesis is essential for the final stages of embryonic development during morphogenesis.

Next, we investigated whether inactivation of cytokinesis mutants late in development affected gut lumen morphogenesis. We evaluated the formation of the apical surface of the intestine by staining for the Ezrin-Radixin-Moesin homologue, ERM-1 (van Furden et al., 2004). The *air-2(or207ts)* mutant fails cytokinesis within minutes after shifting to non-permissive temperature in one-cell embryos (Severson et al., 2000), but does not show penetrant cytokinesis failures unless shifted several hours in older embryos (Figure 4). In comparison, *zen-4 (or153ts)* and *spd-1 (oj5ts)* have similar rapid inactivation kinetics at all stages tested, with *zen-4 (or153ts)* causing penetrant cytokinesis defects while *spd-1 (oj5ts)* does not (data not shown). Therefore, we shifted mutant embryos around the transition between the E4-E8 stages to 26 °C and fixed at the bean stage after intestinal polarization (Fig. 4 A, methods). In all cases, ERM-1 was localized to the apical surface of the intestine and pharynx (Fig. 4 B, Fig. S3 A, D). However, ERM-1 staining was broadened, branched and/or discontinuous in *air-2 (or207ts)* embryos (Fig. 4 C-E, H). Disrupted ERM-1 staining was also observed in *air-2 (or207ts)* embryos, which were shifted at E4-E8 for 4.5-5 hours until the comma stage, indicating that these defects are not resolved later in development (Fig. S3 B, D). Furthermore, the intestine was highly mispositioned within the embryo as revealed by color-coded max Z-projections (Figure 4 I) and the nuclei were often randomly positioned on the z-axis compared with wild-type (Fig. 4 B, E-F inserts). The localization of other apical markers, such as PAR-3, DLG-1 and IFB-2, were similarly disrupted (Fig. S3 E-J, DLG-1 and IFB-2 data not shown). The *zen-4 (or153ts)* embryos shifted from the E4 stage for 2.5-3 hours until the bean stage also had highly penetrant branched and discontinuous apical ERM-1 staining that was mispositioned within the embryo at a lower rate than the *air-2 (or207ts)* mutants (Fig. 4 F, H and Fig. S3 C-D). The *spd-1 (oj5ts)* embryos shifted to 26 °C at E4-E8 until

the E16-E20 stage displayed a significant, but lower rate of lumen defects (Fig. 4 G-I) despite having no lethality (Table 1) and minimal cytokinesis failures. Therefore, we conclude that proper execution of cytokinesis is required for normal lumen formation in the gut.

Cytokinesis in the pharynx: apical midbody migration and AIR-2 accumulation

We also noticed migration of the midbody and accumulation of midbody proteins at the apical surface during the terminal divisions in the pharynx. Unlike the intestine, which originates from a single blastomere that undergoes a very well defined series of divisions, the pharynx has a more complicated structure, containing more than 80 pharyngeal precursor cells (PPCs) that arise from both AB and MS founder cells (Sulston et al., 1983). The PPCs organize into a double plate structure prior to the final division, which occurs at around 310-325 minutes after the first cleavage, and then polarize and undergo apical constriction to become wedge shaped cells that form a lumen by 355 minutes (Rasmussen et al., 2013; Rasmussen et al., 2012). To obtain optimal images of this large, complex structure, we filmed at least a 15-micron Z-depth section of the embryo from both dorsal and ventral aspects with confocal microscopy (Figure 5, Video S6). We also filmed whole embryos with lattice light sheet microscopy, which provides higher spatial resolution during the pharyngeal cell division (Video S7). Similar to our observations in the intestine, PPCs are in the final stages of cell division as they polarize, which has not been previously described. PPCs undergo a symmetric furrowing event that yields a centrally placed midbody between the two daughter cells (Fig. 5 A-C, F, G-H, K, L-M, P and Video S6). Also similar to the intestine, PPC midbodies migrate from their central position between daughter cells to the apical midline of the forming pharyngeal bulb (Fig. 5 D, F, I, K, N, P and Video S6). In PPC terminal divisions, AIR-2::GFP appears as a midbody flank structure that migrates to the apical midline and persists at the apical surface after cyst formation (Fig. 5 D, E, F and Video S6). Similar to AIR-2, RAB-11 and tubulin accumulate and remain localized to the apical surface after polarization (Fig. S4 A-F). We confirmed this localization with staining and show that endogenous AIR-2 can be observed on the apical surface of the pharynx (Fig. S1 H-J). AIR-2 partially co-localized with PAR-6 at the apical membrane, which also acquires γ-tubulin::GFP after polarization (Fig. S4 G-L). ZEN-4::GFP appears on midbodies, migrates to the apical surface, and is rapidly degraded, similar to the intestinal

divisions (Fig. 5 J and Video S6). NMY-2::GFP also labels midbodies and moves to the apical surface, but is recruited to the apical surface during apical constriction (Fig. 5 O, P and Video S6) (Rasmussen et al., 2012). Cytokinesis in the gut and pharynx show similar patterns where midbodies migrate to the apical midline and specific midbody components, especially AIR-2, remain localized at the apical cortex even after the midbody ring is removed. Therefore, similar patterns of apical localization and midbody migration are observed during epithelial polarization in the intestine and pharynx in *C. elegans*.

Dendrites of sensilla neurons: clustering of midbody components

The *C. elegans* amphid sensilla are a sensory organ that contains 12 neurons with dendrites that extend processes through the cuticle and two sheath cells. During morphogenesis, amphid neurons bundle together, anchor at the tip of the animal and migrate back to extend dendrites (Heiman and Shaham, 2009). From the lineage of the 12 sensilla neurons, there are 10 precursor cell divisions that occur between 280 and 400 minutes after the first cleavage (Sulston et al., 1983). These terminal divisions include two daughter cell pairs (ADF/AWB and ASG/AWA) and several where one daughter differentiates into a sensilla neuron while the other daughter undergoes apoptosis (ADL, ASE, ASK, ASI), or differentiates into another neuron (AWC, ASH, AFD, ASJ). Our observations show that these cells undergo a unique form of cytokinesis just before they undergo dendrite morphogenesis (Fig. 6 A). These cells undergo a symmetrical furrowing event before midbodies form centrally between the daughter cells (Fig. 6 B and Video S8-9). A group of at least 6 daughter cell pairs divide initially forming multiple midbodies as observed with both confocal and lattice light sheet imaging (Fig. 6 C and Video S8-9). These midbodies migrate together into a cluster over a 60-minute time window (Fig. 6 D). AIR-2::GFP, RAB-11 and tubulin persist in these clusters (Fig. 6 D, Fig. S5 A-F and Video S8-9), while ZEN-4::GFP rapidly disappears during the midbody clustering process (Fig. 6 E and Video S8). Endogenous AIR-2 can be observed in these lateral apical clusters (Fig. S1 K-M). We observe PAR-6 at the tip of the sensilla cluster, indicating that it is the apical surface of these cells, which accumulates γ-tubulin::GFP similar to the pharynx and gut (Fig. 6 G, Fig. S5 G-L). In contrast to ZEN-4::GFP, NMY-2::GFP migrates with the midbody to the cluster and persists at the very tip of the dendrites (Fig. 6 F

and Video S8). To our knowledge, this is the first detailed examination of the division and initial steps of organization of these neuronal cell precursors.

After formation of the cluster, we observe this apical region move and extend anteriorly until it reaches the tip as the animal progresses from the bean stage through the late comma stage. AIR-2 remains localized along a substantial increasing length of the dendritic extension during the entire elongation process, as does tubulin (Fig. 6 H-J, Fig. S5 J-K, M-O and Video S10). As the amphid dendrites extend from the lateral sides of the embryo, other foci of AIR-2 form within the anterior region of the embryo and migrate toward the tip until six sensilla appear at the anterior tip (Fig. 6 J inset, and Video S10). Although the individual cell divisions cannot be easily discerned in this crowded anterior region, these data suggest that the sensilla in the tip of the animal form through a similar process. These results demonstrate that directly after cytokinesis a midbody migration event brings several midbody components to the apical tip of the amphid dendrites, which remain localized there as dendrite extension occurs. Neuronal cell polarization has been suggested to share mechanisms with epithelial morphogenesis (McLachlan and Heiman, 2013), suggesting that these modified cytokinesis events may play a role in cells that undergo epithelial polarization. Therefore, the midbody migrates from its original position at the end of furrowing to the apical surface in several developing tissues during morphogenesis. Interestingly, AIR-2 remains localized at the apical surface of these tissues well after cytokinesis has occurred.

Amphid sensilla defects in cytokinesis mutants

Lastly, we investigated whether the developing sensory neurons formed normally in temperature sensitive cytokinesis mutants. *C. elegans* amphid neurons can take up lipophilic dyes such as DiI when they form properly and generate cilia that are exposed to the environment (Hedgecock and White, 1985; Perkins et al., 1986). We maintained embryos at the permissive temperature (15 °C) and shifted them to the non-permissive temperature at different embryo stages until they hatched, then we stained the surviving L1 larvae with DiI. In wild-type, amphid neuron cell bodies, amphid dendrites, and phasmid neurons were clearly labeled by DiI and appeared normal as expected (Fig. 7 A). In the *air-2 (or207ts)* mutant, we observed numerous defects in the subset of surviving embryos that did not fail to hatch and became L1 larvae (Fig. 7 B-E). Animals with no observed DiI staining were more common under

longer inactivating conditions (Table 2). All *zen-4 (or153ts)* fail to hatch when shifted during E4-E8, preventing analysis of DiI staining (Table 2). When shifted from the E8 stage, the few surviving *zen-4 (or153ts)* larvae show severe DiI staining defects, which was dramatically reduced if embryos were shifted after the final divisions at the comma-1.5 fold stage (Fig. 7 F, Table 2). The *spd-1 (oj5ts)* animals still had weak defects revealed by DiI staining despite having minimal cytokinesis failures, but never showed a complete lack of staining (Fig. 7I, Table 2). These data are consistent with the hypothesis that proper execution of cytokinesis contributes to proper neurite development. Therefore, cytokinesis and AIR-2 function especially are required late in embryo development for proper morphogenesis of the apical lumen of the gut and proper formation of the sensilla neurons.

Discussion

Our results have revealed complex and reproducible patterns of cytokinesis during the invariant embryonic divisions in *C. elegans.* The entire invariant lineage has been known for several decades and our results suggest that cytokinesis also follows a specific pattern during the lineage. We observe reproducible alterations to furrow symmetry, central spindle length, abscission timing, midbody movement and inheritance. The traditional view of the embryo lineage is that cells are born and subsequently undergo changes that produce the differentiated organization within a tissue. However, our data demonstrate that cells in multiple tissues are completing cytokinesis when they polarize during morphogenesis, which may impact the regulation of the underlying cellular events. This role for cytokinesis might explain why many cells, including several of the amphid neuronal precursors, divide and produce one daughter cell that undergoes apoptosis instead of finishing the divisions earlier when the right number of cells are generated. A modified cytokinesis in the Q neuroblast generates a smaller daughter cell that undergoes apoptosis, which is prevented if the parameters of cytokinesis change (Ou et al., 2010). Given that the entire cell is reconfigured during mitosis and that cytokinesis is the transition period back into the interphase state, this is an ideal time window to reorganize cellular architecture. Understanding how the developmental plasticity of cytokinesis is regulated will be a fascinating question for future studies.

We observe consistent changes to the symmetry of furrow ingression where the first mitosis is relatively symmetric and the second mitosis is highly asymmetric. Previously, the furrow asymmetry in the first division was shown to be a consequence of asymmetric accumulation of contractile ring components during ingression (Maddox et al., 2007). The adhesion between cells may also reinforce this asymmetry to drive the highly asymmetric furrow observed in the second round of divisions (Padmanabhan and Zaidel-Bar, 2017). Whether due to cell intrinsic or extrinsic factors, the asymmetric furrows have previously been postulated to drive efficient furrowing or help maintain proper cell-cell contacts during cytokinesis (Maddox et al., 2007; Morais-de-Sa and Sunkel, 2013). Our data suggest another hypothesis: the asymmetric furrow may be required for the AB midbody to be engulfed by EMS instead of either daughter cell. Given that the midbody has been proposed to deliver signals to cells that inherit it, it is worth noting that the MS cell collects up to four midbodies over time (Singh and Pohl, 2014). Unexpectedly, we see relatively symmetric furrowing in several tissues later in morphogenesis. An asymmetric furrow would be sufficient to position the midbody at the nascent apical surface. Given that the polarization mechanisms are not completely understood, for example the extracellular matrix component laminin is required in the pharynx but not the intestine (Rasmussen et al., 2012), the symmetrical furrow followed by midbody migration may be important for defining and positioning the apical surface. Perhaps there is no good reference for an asymmetric furrow to position the midbody at the apical surface prior to epithelial polarization in cells in different locations. We hypothesize that lumen formation in the gut and pharynx is analogous to that described in MDCK cells with the formation of a midbody-derived apical-membrane initiation site with the addition of midbody migration for correct positioning of this domain (Li et al., 2014).

The coordinated, directed movement of the midbody we observe in several tissues represents a new phenomenon during cytokinesis. Our data also suggest that abscission has not taken place before the midbody migrates in the intestine. This would mean that the two daughter cells polarize while connected at the midbody, which might facilitate their reorganization. These data are somewhat different from what is observed in already polarized epithelia where the furrow constricts from the basal to the apical surface to position the midbody. It is tempting to consider that performing cytokinesis in this particular fashion has an important function in the

polarization process. Since these cells are undergoing a mesenchymal to epithelial transition, it is worth considering whether cytokinesis may have some general function in executing this process. Previously, midbodies have been shown to reposition after forming under normal or mutant conditions (Bernabe-Rubio et al., 2016; Herszterg et al., 2013; Morais-de-Sa and Sunkel, 2013; Singh and Pohl, 2014), but this phenomena is only appreciated in isolated cases and poorly understood. The entire cortex is controlled by several actin cytoskeletal regulators in order to perform cytokinesis (Jordan and Canman, 2012), perhaps this is also employed to control the movement of the midbody. In the future, it will be important to investigate how the midbody moves to the apical surface after furrowing is completed.

In the tissues we investigated, the cells are undergoing their terminal cell division before morphogenesis, although some cells like those in the gut undergo post-embryonic divisions. These cells are also undergoing epithelial polarization and a mesenchymal to epithelial transition. After midbody movement, RAB-11, AIR-2 and possibly other molecules are recruited to the apical surface. Certainly, these different tissues have unique gene expression programs, part of which might involve proteins delivered to the midbody and the apical surface. A transmembrane protein that binds to an extracellular partner is expressed in the tip of the dendrites in amphid sensilla, which is required to maintain dendrite attachment at the tip of the embryo (Heiman and Shaham, 2009). It is unknown how this protein localizes to the tip of the dendrite, but one speculative possibility is that it could be delivered through cytokinesis-directed membrane trafficking. A stem cell marker protein is released in extracellular membrane particles by neuroepithelial cells from the cilium and midbody, showing a similarity between these two organelles (Dubreuil et al., 2007). Later in life, the worm releases exosomes from the sensory cilia that form at the tip of the dendrites of the sensilla for communication between animals (Wang et al., 2014a). Perhaps the initial secretory apparatus built during cytokinesis to promote cell division is recruited to the apical surface of these neurons to recruit machinery involved in exosome release. Further investigation is required to define the molecular contributions provided by the midbody to the apical surface of these tissues.

Once the midbody moves to the apical surface, we observe that different components of the midbody have different fates, which is an unexpected and novel observation. Typically, once the midbody is abscised from the cell, it is thought that

most midbody proteins are discarded with the remnant, as observed in the early embryo divisions. Aurora B kinase remains at the apical surface well after other midbody components like ZEN-4 are removed. The limit of the resolution of light microscopy does not allow us to characterize in detail how this occurs. The most likely model is that the midbody is cut from the plasma membrane and flanking proteins like Aurora B, RAB-11, and microtubules are left behind. Among the many mitotic functions of Aurora B, it is a critical regulator of the timing of abscission (Mathieu et al., 2013; Steigemann et al., 2009). Based on our observations of midbody flank microtubules, abscission may occur after the midbody migration event, and the delay in abscission might require Aurora B activity. Inhibition of Aurora B kinase in mouse embryos caused the loss of midbody derived interphase bridges and a reduction of RAB-11 and cell adhesion molecules delivered to apical membranes (Zenker et al., 2017). Aurora B also regulates a number of cytoskeletal regulators during cytokinesis that control cell shape (Ferreira et al., 2013; Floyd et al., 2013; Goto et al., 2003; Kettenbach et al., 2011), and it will be important to determine whether any are involved with the events we observed. In the intestine, the central spindle elongates dramatically as the midbody migrates, which might also be regulated by Aurora B (Bastos et al., 2013). Along these lines, altered expression of the central spindle protein PRC-1 (the homologue of *spd-1*) contributes to variant midzone microtubule density in different tissues in the *Xenopus* embryo, which correlates with changes to furrow ingression and midbody behavior (Kieserman et al., 2008). While we observe the centralspindlin component ZEN-4 becoming internalized and degraded in the three tissues, it was previously implicated in morphogenesis of the epidermis and pharynx (Hardin et al., 2008; Portereiko et al., 2004; Von Stetina et al., 2017). It remains to be determined whether this role is related to the dynamics of cytokinesis or a cytokinesis-independent function of ZEN-4 as previously suggested. Therefore, further study will be required to understand the role of the central spindle components during the specialized cytokinesis events that occur during morphogenesis.

In the sensilla, the centriole moves to the tip of the dendrite to form the base of the sensory cilia of these neurons (Dammermann et al., 2009; Nechipurenko et al., 2017; Perkins et al., 1986). Multiple central spindle proteins localize to the base of cilia in *Xenopus* epithelial cells and are required for cilia morphology after the divisions are completed in *C. elegans* (Kieserman et al., 2008; Smith et al., 2011).

Additionally, loss of Aurora B kinase causes aberrant neuronal axon morphology, and overexpression of Aurora B causes extended axonal outgrowth in zebrafish (Gwee et al., 2018). At the apical surface of the gut, γ-tubulin and other pericentriolar material is delivered from the centrosome while the centrioles are discarded. The gut apical membrane ultimately becomes elaborated with microvilli (Feldman and Priess, 2012; Leung et al., 1999). We also observed γ-tubulin at the apical surface of the pharynx and sensilla dendrites. Therefore, different material provided by the midbody and centrosome may contribute to the cytoskeletal architecture of the apical surface. Delineating the precise relationship between these two organelles and deciphering how cytokinesis contributes to proper cellular reorganization during morphogenesis will be a major focus of future studies.

Acknowledgements

Lattice light sheet microscopy was performed in collaboration with the Advanced Imaging Center at HHMI Janelia Research Campus, a facility jointly supported by the Gordon and Betty Moore Foundation and the Howard Hughes Medical Institute. We appreciate the CGC and Wormbase funded by the NIH Office of Research Infrastructure Programs (P40 OD010440) and National Human Genome Research Institute (U41 HG002223), which provided some *C. elegans* strains and genome information. We are grateful to members of the Bembenek laboratory for productive discussion, reagent preparation and handling strains. We also thank Dr. Max Heiman, Dr. Zhirong Bao for discussions and Dr. Don Fox, Dr. John White, Dr. John Heddleston, Dr. Heidi Hehnley-Chang, Lindsay Rathbun, and Erica Colicino for critical feedback on the manuscript.

Figure Legends

Figure 1. Cytokinesis in the first two mitotic divisions

(A) Illustration of cytokinesis in the first two mitotic divisions indicating the invariant fate of the midbody after division. Orange arrowheads indicate the first midbody, while blue arrowheads indicate the AB midbody. (B-F) Cytokinesis labeled with AIR-2::GFP (green) and PH::mCherry (magenta), H2B::mCherry (magenta). During late anaphase, Aurora B localizes on the central spindle (B) which condenses into the midbody flank (C, orange arrowhead) and remains on the midbody until it is internalized by the AB daughter cell (D, orange arrowhead). During the second mitosis, the furrow is highly asymmetric and sweeps the central spindle against the EMS boundary, where the midbody forms (E, blue arrowhead). EMS engulfs the midbody instead of either of the AB daughter cells (F, blue arrowhead). (G-K) NMY-2::GFP (green) and PH::mCherry (magenta) show localization to the furrow (G) and midbody ring (H-K). (L-P) ZEN-4::GFP (green) appears on the central spindle (L) and the midbody (M-P). (Q-U) RAB-11::mCherry (green) co-localized with AIR-2::GFP (magenta) briefly at the midbody, but does not remain on the midbody once it is internalized into cytosol (R-U). (V-X) Quantification of furrow asymmetry, measurement illustrated in V, W. (X) Asymmetry parameter is significantly greater in second cell division. Scale bar, 10 μm.

Figure 2. Cytokinesis in the E8-E16 intestinal divisions

(A) Diagram of cytokinesis in the intestinal E8-E16 mitotic divisions indicating localization of Aurora B (green, midbody ring in magenta) (B-D) Lattice light sheet imaging of E8-E16 intestinal cell divisions in embryos expressing AIR-2::GFP (green) with PH::mCherry (magenta). AIR-2::GFP labels midbodies (labeled 1-8 in B) in the middle of daughter cell pairs, which migrate (arrowheads, C) to the nascent apical membrane where it persists well after polarization is complete (time shown in minutes:seconds bottom left). (E-G) Spinning disc confocal microscopy of AIR-2::GFP (green) with H2B::mCherry (magenta) and PH::mCherry, (magenta, time shown in minutes:seconds bottom left). (H) Image series of Epla division with AIR-2::GFP (green, PH::mCherry, magenta) starting in prometaphase, clearly indicating midbody formation and migration to apical midline. (I-K) NMY-2 (green) localizes to furrows, then midbody rings (labeled 1-8 in F) that move to the midline (arrowheads, J) but do not persist (rectangle box in K). (L) Montage showing a single NMY-2::GFP labeled midbody migrating to midline. (M-N) Single plane imaging of midbody dynamics in individual intestine cell shows extension of the central spindle and apical membrane localization of AIR-2::GFP (M) and rapid internalization of ZEN-4::GFP (N) to the cytosol (time in minute: second indicated on right top). (O) Quantification of midline

perdurance of different midbody components (measured from the end of furrowing to internalization or loss of signal). (P) Illustration of E8 division and (Q) quantification of the ratio of maximal midbody flank length to cell length. Scale bar, 10 μm. Error bars indicate standard deviation of the mean.

Figure 3. Comparison of central spindle microtubule dynamics

Imaging of microtubule dynamics during different cell divisions to visualize central spindle and midbody flank microtubules. (A-B) AIR-2::GFP (magenta) and β-tubulin TBB-1::mCherry (green) colocalize at the central spindle during anaphase and furrowing in the first cell division. AIR-2::GFP persists at the midbody after microtubules are lost, which correlates closely with abscission timing (B). (C-D) AIR-2::GFP (magenta) and β-tubulin TBB-1::mCherry (green) colocalize on the central spindle adjacent to EMS after highly asymmetric furrowing. Microtubules are lost in a similar amount of time as the first division (D). (E-G) Tubulin TBB-1::mCherry (green) and AIR-2::GFP (magenta) localize to an extended flank region during intestinal midbody migration (F, arrowheads). (G) Tubulin and AIR-2 persist at the apical membrane after polarization (rectangle box). (H) Single z-plane imaging of midbody flank microtubules (arrowheads) from the dorsal aspect during Epra cell division and midbody migration. The extended flanking microtubules persist at least 3 times longer than earlier divisions throughout the migration process until they can no longer be distinguished from other microtubules at the apical surface. (I) Quantification of tubulin persistence time at the central spindle during different cell divisions. Scale bar, 10 μm. Error bars indicated standard deviation of the mean.

Figure 4. **Cytokinesis mutants have disrupted intestinal morphogenesis**

Shifting temperature-sensitive cytokinesis mutants to 25 °C at the E4-E8 stage until they reach the bean stage causes severe lumen defects in the intestine. (A) Timeline of cell division events in the intestine emphasizing E4-E8 timing and E8-E16 cytokinesis and the timing of temperature shift experiments. (B) ERM-1 staining in wild type bean stage embryos is enriched at the apical midline of the intestine (dotted rectangle). Maximum z-projected images color-coded according to Z-depth (using FIJI temporal-color code plugin, scale shown in I) to visualize the three-dimensional position of ERM-1 and nuclei (B-G, I). In *air-2(or207ts)*, multiple defects are observed, including mispositioning of the entire intestine (C-E), branches in the apical surface (C), gaps in the apical surface creating a discontinuous lumen (D), or broader staining of ERM-1 (E). (F) The *zen-4(or153ts)* mutant causes many of

these phenotypes, including branching of the apical surface. (G) There are subtle lumen and nuclei position defects in *spd-1(oj5ts)* embryos. (H) Quantification of apical defects observed by ERM-1 staining in the different mutants. (I) Quantification of the defective z-plane distribution of the apical surface in the different mutants. The more colors a lumen has in the projection, the more skewed in the Z-axis it is within the embryo. Scale bar, 10 μm.

Figure 5. Cytokinesis During Pharyngeal Precursor Cell Polarization

(A) Illustration of the mesenchymal to epithelial transition of pharyngeal precursor cells (PPCs) showing cell division and dynamics of Aurora B (green, midbody ring in magenta). (B-E) PPC division labeled with AIR-2::GFP (green, H2B::mCherry in magenta) from both ventral (B-D) and dorsal (E) views. AIR-2::GFP localizes to chromatin in metaphase (B) and moves to the central spindle in anaphase (C) and appears on the midbody which moves toward the midline (D). AIR-2 persists at the apical surface for an extended time (E, time in minutes:seconds indicated below). (F) Image series showing an AIR-2::GFP labeled midbody migrating toward the midline. Imaging two different midbody ring components, (G-K) ZEN-4 (green, TBB-1::mCherry in magenta) and (L-P) NMY-2 (green, TBB-1::mCherry in magenta), shows the movement of the midbody to the midline (I, N). ZEN-4 does not persist (J, arrowheads indicate internalized midbodies not yet degraded), while NMY-2 accumulates at the apical midline during apical constriction (O). Time shown in minutes: seconds. Scale bar, 10 μm.

Figure 6. **Midbody components label dendrites of sensilla neurons**

(A) Diagram of sensilla precursor cell (SPC) divisions and the localization of the AIR-2::GFP at the midbody during cytokinesis until the apical clustering during polarization. (B-D) Cytokinesis in SPCs in the anterior lateral region of the embryo expressing AIR-2::GFP (green, H2B::Cherry in magenta) gives rise to multiple midbodies (arrowheads B,C) that cluster together at the lateral sides of the embryos (D). (E) The midbody ring marker ZEN-4::GFP (green, microtubules in magenta) is internalized and degraded before the cluster forms, which is also concentrated with microtubules (arrowheads). (F) NMY-2::GFP (green, microtubules in magenta) localizes to midbodies that cluster and remain at the tip as the dendrite extension forms. (G) PAR-6::mCherry (green, AIR-2::GFP in magenta) localizes to tip of the cluster (arrowheads) and persists at the tip of the dendrites as they extend, indicating that this is the apical surface of these cells. (H-J) After the apical surface cluster forms, AIR-2::GFP remains at the tip (red arrowheads) as the cells migrate to the nose of the animal. AIR-

2::GFP also labels a substantial portion of the length of the dendrite as they extend (J). Insert in (J) is a rotated max z-projection showing the anterior end of the animal after multiple sensilla form (J). Time shown in minutes:seconds. Scale bar, 10 μm.

Figure 7. **Cytokinesis mutants have disrupted sensilla neuron morphogenesis**

(A-E) Visualizing dendrite and neuron morphology by DiI staining in surviving larvae after shifting mutants to 25 °C at the E4 or E8 stage until hatching. (A) In wild type animals, two dendrite bundles can be clearly observed as well as amphid and phasmid neurons. (B-E) Hatched mutant larvae displayed a variety of neurite defects, including No-DiI signal (B, F), Weak signal (C, G), dendrite shape and positioning defects (D) and additional diffuse staining throughout the head of the animal (E, H, I).

Materials and Methods

C. elegans Strains

C. elegans strains were maintained with standard protocols. *C. elegans* strains expressing midbody proteins driven by the *pie-1* promoter are listed in Table 2. All temperature-sensitive mutants were obtained from the Caenorhabditis Genetics Center.

Embryo Preparation and Imaging

For live imaging, young gravid hermaphrodites were dissected in M9 buffer containing polystyrene microspheres and sealed between two coverslips with vaseline (Pohl and Bao, 2010). Live cell imaging was performed on a spinning disk confocal system that uses a Nikon Eclipse inverted microscope with a 60 X 1.40NA objective, a CSU-22 spinning disc system, and a Photometrics EM-CCD camera from Visitech International. Images were acquired by Metamorph (Molecular Devices) and analyzed by ImageJ/FIJI Bio-Formats plugins (National Institutes of Health) (Linkert et al., 2010; Schindelin et al., 2012). Whole embryo live imaging was performed on a lattice light sheet microscopes housed in the Eric Betzig lab, Bi-Chang Chen lab, or the Advanced Imaging Center at HHMI Janelia. The system is configured and operated as previously described (Chen et al., 2014). Briefly, embryos were dissected out and adhered to 5 mm round glass coverslips (Warner Instruments, Catalog # CS-5R). Samples were illuminated by lattice light-sheet using 488 nm or 560 nm diode lasers (MPB Communications) through an excitation objective (Special Optics, 0.65 NA, 3.74-mm WD). Fluorescent emission was collected by detection objective (Nikon, CFI Apo LWD 25XW, 1.1 NA), and detected by a sCMOS camera (Hamamatsu Orca Flash 4.0 v2). Acquired data were deskewed as previously described (Chen et al., 2014) and deconvolved using an iterative Richardson-Lucy algorithm. Point-spread functions for deconvolution were experimentally measured using 200nm tetraspeck beads adhered to 5 mm glass coverslips (Invitrogen, Catalog # T7280) for each excitation wavelength.

Immunostaining Assay in *C. elegans* Embryos

Apical marker staining was performed with the freeze-crack methanol protocol (Leung et al., 1999). Immunostaining with anti-AIR-2 antibodies was performed as described (Schumacher et al., 1998). Primary antibodies and (dilutions) used were

753 anti-ERM-1 (1:200); P4A1/PAR-3 (1:200); DLG-1 (1:200); MH33 (1:150); AIR-2
754 (1:50). 1:200-400 dilutions of Alexa 588 and 468 secondary antibodies were used in
755 the study. To stain temperature-sensitive mutants, two-cell stage embryos were
756 dissected from gravid worms, mounted in 10 μL of M9 buffer, and kept cold on ice.
757 The two-cell stage embryos were incubated at 15 °C for 4-7 hours until specific
758 stages, then shifted to the restrictive temperature (25 °C) for 2-4 hours and stained as
759 described above.
760

761 **DiI staining in *C. elegans***

762 DiI staining of wild-type and temperature sensitive mutants was done as previously
763 described (Tong and Burglin, 2010). Two-cell stage embryos were incubated at 15 °C
764 for 6.5~7 hours until they reached the polarized E16 stage, then shifted to the
765 restrictive temperature (25 °C) with 1:200 dilution of stock DiI dye solution
766 containing 2 mg/mL DiI in dimethyl formamide for 18-24 hours. Hatched larvae were
767 transferred to M9 and washed twice in M9 before mounting in 25 mM levamisole on
768 2% agar pads for imaging.
769

770 **Temperature-Shift Experiments**

771 Temperature-sensitive mutants were maintained at 15 °C. To perform temperature
772 shifts on staged embryos, gravid adults were transferred to a dissection chamber (<
773 4 °C), which was precooled in ice bucket, with 20 μL of ice-cold M9 Buffer. Two-
774 Cell stage embryos were quickly transferred (within a 5-10 minute time window) via
775 mouth pipette (Aspirator tube assemblies, Sigma) to Fisherbrand Hanging Drop Slides
776 (Catalogue #12-560B) on ice. The slide was placed into a humidified chamber and
777 incubated at 15 °C until the appropriate stages were reached and then shifted to 26 °C.
778 Incubation times were determined based on *C. elegans* embryonic lineage timing and
779 adjusted according to DAPI staining to ensure each mutant was shifted at a similar
780 stage of embryo development. To inactivate *air-2 (or207ts)*, mutant embryos were
781 incubated for 5 hours at 15 °C and shifted to 26 °C for 3 hours to reach the bean stage
782 or 5 hours at 26 °C to reach the comma stage. This was the minimum amount of time
783 to shift embryos to non-permissive temperature and observe significant cytokinesis
784 defects by the E8-E16 division, indicating significant reduction of AIR-2 function.
785 Most embryos reached the E4-E8 division at the time of the shift. By live imaging we

found that there was little disruption of the E4-E8 division under these conditions since (n=4/5) *air-2 (or207ts)* embryos have 8 normal E8 cells. N2, *spd-1 (oj5ts)*, and *zen-4 (or153ts)* embryos were incubated for 4.5 hours at 15 °C to reach E4-E8 stage, followed by 3 hours at 26 °C to reach the bean stage and 5 hours at 26 °C to reach the comma stage. To shift embryos at the comma stage, *air-2 (or207ts)* embryos were incubated for 12 hours at 15 °C and N2, *spd-1 (oj5ts) and zen-4 (or153ts)* embryos were incubated 11-11.5 hours at 15 °C.

796 **Table 1. Hatch rate of temperature sensitive mutants.**

797

Stage Before Shifting	Genotype	Hatch Rate % (Hatch Embryos/Total)
15 °C Forever	N2	100% (32/32)
	air-2 (or207ts)	53.6% (37/69)
	zen-4 (or153ts)	100% (28/28)
	spd- (oj5ts)	100% (35/35)
E4-E8	N2	100% (26/26)
	air-2 (or207ts)	6.3% (2/32)
	zen-4 (or153ts)	0% (0/57)
	spd- (oj5ts)	100% (48/48)
E8-E16	N2	100% (45/45)
	air-2 (or207ts)	14.4% (13/90)
	zen-4 (or153ts)	10.1% (10/99)
	spd- (oj5ts)	100% (83/83)
Comma-1.5 Fold	N2	100% (36/36)
	air-2 (or207ts)	33.7% (31/92)
	zen-4 (or153ts)	85.7% (54/63)
	spd- (oj5ts)	100% (27/27)

798

799 **Table 2. Quantification of DiI Staining of Temperature-Sensitive Mutants**

800

Stage Before Shifting	Genotype	No DiI Signal	Weak DiI signal	Shape & Position Defect	Extended DiI Staining
15 °C Forever	N2	0% (0/32)	0% (0/32)	0% (0/32)	0% (0/32)
	air-2(or207ts)	2.7% (1/37)	8.1% (3/37)	2.7% (1/37)	0% (0/37)
	zen-4(or153ts)	0% (0/18)	0% (0/18)	0% (0/18)	0% (0/18)
	spd-1(oj5ts)	0% (0/34)	0% (0/34)	0% (0/34)	0% (0/34)
E4-E8	N2	0% (0/10)	0% (0/10)	0% (0/10)	0% (0/10)
	air-2(or207ts)	50% (1/2)	0% (0/2)	50% (1/2)	0% (0/2)
	zen-4(or153ts)	0% (0/0)	0% (0/0)	0% (0/0)	0% (0/0)
	spd-1(oj5ts)	0% (0/44)	4.5% (2/44)	9.1% (4/44)	6.8% (3/44)
E8-E16	N2	0% (0/29)	0% (0/29)	0% (0/29)	0% (0/29)
	air-2(or207ts)	16.7% (2/12)	58.3% (7/12)	58.3% (7/12)	0% (0/12)
	zen-4(or153ts)	77.8% (7/9)	11.1% (1/9)	22.2% (2/9)	0% (0/9)
	spd-1(oj5ts)	0% (0/59)	0% (0/59)	8.5% (5/59)	5.1% (3/59)
Comma-1.5 Fold	N2	0% (0/21)	0% (0/21)	0% (0/21)	0% (0/21)
	air-2(or207ts)	6.9% (2/29)	10.3% (3/29)	0% (0/29)	13.8% (4/29)
	zen-4(or153ts)	0% (0/53)	0% (0/53)	0% (0/53)	22.6% (12/53)
	spd-1(oj5ts)	0% (0/18)	0% (0/18)	0% (0/18)	33.3% (6/18)

801 **Table 3. Strains used in this study.**

Strain	**Genotype**
N2	Bristol (wild-type)
EKM48	*unc-119(ed3) iii; ojIs51 [Ppie-1::GFP::air-2; unc-119(+)]*
EKM50	*unc-119(ed3) iii; ojIs51 [Ppie-1::GFP::air-2; unc-119(+)]; ItIs37 [Ppie-1::mCherry::his-58 (pAA64); unc-119(+)] iv; ItIs44 [Ppie-1::mCherry::PH (PLC1delta1); unc-119(+)]v*
EKM51	*unc-119(ed3) iii; ojIs51 [Ppie-1::GFP::air-2; unc-119(+)]; ItIs37 [Ppie-1::mCherry::his-58 (pAA64); unc-119(+)] iv*
EKM52	*unc-119(ed3) iii; ojIs51 [Ppie-1::GFP::air-2; unc-119(+)]; ItIs44 [Ppie-1::mCherry::PH (PLC1delta1); unc-119(+)] v*
JAB23	*unc-119(ed3) iii; ojIs51 [Ppie-1::GFP::air-2; unc-119(+)]; weIs21 [pJA138 (pie-1::mCherry::tub)]*
JAB60	*unc-119(ed3) iii; ojIs51 [Ppie-1::GFP::air-2; unc-119(+)]; pwIs476 [Ppie-1::mCherry::rab-11]*
JAB116	*unc-119(ed3) iii; weIs21 [pJA138 (Ppie-1::mCherry::tub)]; unc-119(+)]; zuIs45 [nmy-2::NMY-2::GFP; unc-119(+)] v*
NWG002	*unc-119(ed3) iii; ItIs44 [Ppie-1::mCherry::PH (PLC1delta1); unc-119(+)]v; zuIs45 [nmy-2::NMY-2::GFP; unc-119(+)] v*
JAB24	*zen-4(or153ts) iv; xsEx6 [zen-4::GFP; rol-6 (su1006)]; unc-119(ed3) iii; weIs21 [pJA138 (pie-1::mCherry::tub)]*
JAB34	*zen-4(or153) iv; xsEx6 [zen-4::GFP; rol-6 (su1006)]; unc-119(ed3) iii; ItIs44 [Ppie-1::mCherry::PH (PLC1delta1); unc-119(+)] v*
JAB32	*unc-119(ed3) iii; ddIs26 [Ppie-1::mCherry::T26E3.3; unc-119(+)]v; ojIs51 [Ppie-1::GFP::air-2; unc-119(+)]*
EU630	*air-2(or207) i.*
EU716	*zen-4(or153) iv.*

WH12	*spd-1 (oj5) i.*
WH421	*unc-119(ed3) iii; ojIs51 [Ppie-1::GFP::air-2; unc-119(+)];spd-1 (oj5) i.*
JAB39	*unc-119(ed3) iii; ruls32III;dd156[tbg-1::GFP;unc-119(+)];; ojIs51 [Ppie-1::GFP::air-2; unc-119(+)];spd-1 (oj5) i.*
JAB52	*unc-119(ed3) iii; ruls32III;dd156[tbg-1::GFP;unc-119(+)]; ruls32[Ppi-1::GFP::His-58; unc-119(ed3); weIs21 [pJA138 (pie-1::mCherry::tub)]*

802

Bibliography

Ai, E., Poole, D.S., and Skop, A.R. (2009). Rack-1 Directs Dynactin-dependent RAB-11 Endosomal Recycling during Mitosis in Caenorhabditis elegans (vol 20, 1629, 2009). Mol Biol Cell *20*, 5036-5036.

Albertson, R., Riggs, B., and Sullivan, W. (2005). Membrane traffic: a driving force in cytokinesis. Trends Cell Biol *15*, 92-101.

Amini, R., Goupil, E., Labella, S., Zetka, M., Maddox, A.S., Labbe, J.C., and Chartier, N.T. (2015). C. elegans Anillin proteins regulate intercellular bridge stability and germline syncytial organization (vol 206, pg 129, 2014). J Cell Biol *209*, 467-467.

Bai, X.F., and Bembenek, J.N. (2017). Protease dead separase inhibits chromosome segregation and RAB-11 vesicle trafficking. Cell Cycle *16*, 1902-1917.

Bastos, R.N., Gandhi, S.R., Baron, R.D., Gruneberg, U., Nigg, E.A., and Barr, F.A. (2013). Aurora B suppresses microtubule dynamics and limits central spindle size by locally activating KIF4A. J Cell Biol *202*, 605-621.

Bembenek, J.N., Verbrugghe, K.J.C., Khanikar, J., Csankovszki, G., and Chan, R.C. (2013). Condensin and the Spindle Midzone Prevent Cytokinesis Failure Induced by Chromatin Bridges in C. elegans Embryos. Curr Biol *23*, 937-946.

Bembenek, J.N., White, J.G., and Zheng, Y.X. (2010). A Role for Separase in the Regulation of RAB-11-Positive Vesicles at the Cleavage Furrow and Midbody. Curr Biol *20*, 259-264.

Bernabe-Rubio, M., Andres, G., Casares-Arias, J., Fernandez-Barrera, J., Rangel, L., Reglero-Real, N., Gershlick, D.C., Fernandez, J.J., Millan, J., Correas, I., *et al.* (2016). Novel role for the midbody in primary ciliogenesis by polarized epithelial cells. J Cell Biol *214*, 259-273.

Bringmann, H., and Hyman, A.A. (2005). A cytokinesis furrow is positioned by two consecutive signals. Nature *436*, 731-734.

Canman, J.C., Hoffman, D.B., and Salmon, E.D. (2000). The role of pre- and post-anaphase microtubules in the cytokinesis phase of the cell cycle. Curr Biol *10*, 611-614.

Carlton, J.G., Caballe, A., Agromayor, M., Kloc, M., and Martin-Serrano, J. (2012). ESCRT-III Governs the Aurora B-Mediated Abscission Checkpoint Through CHMP4C. Science *336*, 220-225.

Carmena, M., Earnshaw, W.C., and Glover, D.M. (2015). The Dawn of Aurora Kinase Research: From Fly Genetics to the Clinic. Front Cell Dev Biol *3*, 73.

Chen, B.C., Legant, W.R., Wang, K., Shao, L., Milkie, D.E., Davidson, M.W., Janetopoulos, C., Wu, X.F.S., Hammer, J.A., Liu, Z., *et al.* (2014). Lattice light-sheet microscopy: Imaging molecules to embryos at high spatiotemporal resolution. Science *346*, 439-+.

Chen, C.T., Ettinger, A.W., Huttner, W.B., and Doxsey, S.J. (2013). Resurrecting remnants: the lives of post-mitotic midbodies. Trends Cell Biol *23*, 118-128.

Crowell, E.F., Gaffuri, A.L., Gayraud-Morel, B., Tajbakhsh, S., and Echard, A. (2014). Engulfment of the midbody remnant after cytokinesis in mammalian cells. J Cell Sci *127*, 3840-3851.

Dammermann, A., Pemble, H., Mitchell, B.J., McLeod, I., Yates, J.R., Kintner, C., Desai, A.B., and Oegema, K. (2009). The hydrolethalus syndrome protein HYLS-1 links core centriole structure to cilia formation. Gene Dev *23*, 2046-2059.

Dubreuil, V., Marzesco, A.M., Corbeil, D., Huttner, W.B., and Wilsch-Brauninger, M. (2007). Midbody and primary cilium of neural progenitors release extracellular membrane particles enriched in the stem cell marker prominin-1. J Cell Biol *176*, 483-495.

Eggert, U.S., Mitchison, T.J., and Field, C.M. (2006). Animal cytokinesis: From parts list to mechanisms. Annu Rev Biochem *75*, 543-566.

El Amine, N., Kechad, A., Jananji, S., and Hickson, G.R. (2013). Opposing actions of septins and Sticky on Anillin promote the transition from contractile to midbody ring. J Cell Biol *203*, 487-504.

Ettinger, A.W., Wilsch-Brauninger, M., Marzesco, A.M., Bickle, M., Lohmann, A., Maliga, Z., Karbanova, J., Corbeil, D., Hyman, A.A., and Huttner, W.B. (2011). Proliferating versus

855 differentiating stem and cancer cells exhibit distinct midbody-release behaviour. Nat
856 Commun *2*, 503.
857 Feldman, J.L., and Priess, J.R. (2012). A role for the centrosome and PAR-3 in the hand-off
858 of MTOC function during epithelial polarization. Curr Biol *22*, 575-582.
859 Ferreira, J.G., Pereira, A.J., Akhmanova, A., and Maiato, H. (2013). Aurora B spatially
860 regulates EB3 phosphorylation to coordinate daughter cell adhesion with cytokinesis. J Cell
861 Biol *201*, 709-724.
862 Floyd, S., Whiffin, N., Gavilan, M.P., Kutscheidt, S., De Luca, M., Marcozzi, C., Min, M.,
863 Watkins, J., Chung, K., Fackler, O.T., *et al.* (2013). Spatiotemporal organization of Aurora-B
864 by APC/CCdh1 after mitosis coordinates cell spreading through FHOD1. J Cell Sci *126*,
865 2845-2856.
866 Fox, D.T., and Duronio, R.J. (2013). Endoreplication and polyploidy: insights into
867 development and disease. Development *140*, 3-12.
868 Goto, H., Yasui, Y., Kawajiri, A., Nigg, E.A., Terada, Y., Tatsuka, M., Nagata, K., and
869 Inagaki, M. (2003). Aurora-B regulates the cleavage furrow-specific vimentin
870 phosphorylation in the cytokinetic process. J Biol Chem *278*, 8526-8530.
871 Green, R.A., Mayers, J.R., Wang, S., Lewellyn, L., Desai, A., Audhya, A., and Oegema, K.
872 (2013). The midbody ring scaffolds the abscission machinery in the absence of midbody
873 microtubules. J Cell Biol *203*, 505-520.
874 Green, R.A., Paluch, E., and Oegema, K. (2012). Cytokinesis in Animal Cells. Annu Rev Cell
875 Dev Bi *28*, 29-+.
876 Greenbaum, M.P., Ma, L., and Matzuk, M.M. (2007). Conversion of midbodies into germ cell
877 intercellular bridges. Developmental Biology *305*, 389-396.
878 Guizetti, J., Schermelleh, L., Mantler, J., Maar, S., Poser, I., Leonhardt, H., Muller-Reichert,
879 T., and Gerlich, D.W. (2011). Cortical constriction during abscission involves helices of
880 ESCRT-III-dependent filaments. Science *331*, 1616-1620.
881 Gwee, S.S.L., Radford, R.A.W., Chow, S., Syal, M.D., Morsch, M., Formella, I., Lee, A.,
882 Don, E.K., Badrock, A.P., Cole, N.J., *et al.* (2018). Aurora kinase B regulates axonal
883 outgrowth and regeneration in the spinal motor neurons of developing zebrafish. Cell Mol
884 Life Sci.
885 Haglund, K., Nezis, I.P., and Stenmark, H. (2011). Structure and functions of stable
886 intercellular bridges formed by incomplete cytokinesis during development. Commun Integr
887 Biol *4*, 1-9.
888 Hardin, J., King, R., Thomas-Virnig, C., and Raich, W.B. (2008). Zygotic loss of ZEN-
889 4/MKLP1 results in disruption of epidermal morphogenesis in the C. elegans embryo. Dev
890 Dyn *237*, 830-836.
891 Hedgecock, E.M., and White, J.G. (1985). Polyploid Tissues in the Nematode
892 Caenorhabditis-Elegans. Developmental Biology *107*, 128-133.
893 Heiman, M.G., and Shaham, S. (2009). DEX-1 and DYF-7 establish sensory dendrite length
894 by anchoring dendritic tips during cell migration. Cell *137*, 344-355.
895 Herszterg, S., Leibfried, A., Bosveld, F., Martin, C., and Bellaiche, Y. (2013). Interplay
896 between the Dividing Cell and Its Neighbors Regulates Adherens Junction Formation during
897 Cytokinesis in Epithelial Tissue. Dev Cell *24*, 256-270.
898 Herszterg, S., Pinheiro, D., and Bellaiche, Y. (2014). A multicellular view of cytokinesis in
899 epithelial tissue. Trends Cell Biol *24*, 285-293.
900 Hime, G.R., Brill, J.A., and Fuller, M.T. (1996). Assembly of ring canals in the male germ
901 line from structural components of the contractile ring. Journal of Cell Science *109*, 2779-
902 2788.
903 Hu, C.K., Coughlin, M., and Mitchison, T.J. (2012). Midbody assembly and its regulation
904 during cytokinesis. Mol Biol Cell *23*, 1024-1034.
905 Jordan, S.N., and Canman, J.C. (2012). Rho GTPases in Animal Cell Cytokinesis: An
906 Occupation by the One Percent. Cytoskeleton *69*, 919-930.
907 Kettenbach, A.N., Schweppe, D.K., Faherty, B.K., Pechenick, D., Pletnev, A.A., and Gerber,
908 S.A. (2011). Quantitative Phosphoproteomics Identifies Substrates and Functional Modules of
909 Aurora and Polo-Like Kinase Activities in Mitotic Cells. Sci Signal *4*.

Kieserman, E.K., Glotzer, M., and Wallingford, J.B. (2008). Developmental regulation of central spindle assembly and cytokinesis during vertebrate embryogenesis. Curr Biol *18*, 116-123.

Konig, J., Frankel, E.B., Audhya, A., and Muller-Reichert, T. (2017). Membrane remodeling during embryonic abscission in Caenorhabditis elegans. J Cell Biol.

Lacroix, B., and Maddox, A.S. (2012). Cytokinesis, ploidy and aneuploidy. J Pathol *226*, 338-351.

Leung, B., Hermann, G.J., and Priess, J.R. (1999). Organogenesis of the Caenorhabditis elegans intestine. Dev Biol *216*, 114-134.

Li, D.Y., Mangan, A., Cicchini, L., Margolis, B., and Prekeris, R. (2014). FIP5 phosphorylation during mitosis regulates apical trafficking and lumenogenesis. Embo Rep *15*, 428-437.

Li, R. (2007). Cytokinesis in development and disease: variations on a common theme. Cell Mol Life Sci *64*, 3044-3058.

Linkert, M., Rueden, C.T., Allan, C., Burel, J.M., Moore, W., Patterson, A., Loranger, B., Moore, J., Neves, C., MacDonald, D., *et al.* (2010). Metadata matters: access to image data in the real world. J Cell Biol *189*, 777-782.

Lujan, P., Varsano, G., Rubio, T., Hennrich, M.L., Sachsenheimer, T., Galvez-Santisteban, M., Martin-Belmonte, F., Gavin, A.C., Brugger, B., and Kohn, M. (2016). Phosphatase of regenerating liver (PRL)-3 disrupts epithelial architecture by altering the post-mitotic midbody position. J Cell Sci.

Maddox, A.S., Habermann, B., Desai, A., and Oegema, K. (2005). Distinct roles for two C-elegans anillins in the gonad and early embryo. Development *132*, 2837-2848.

Maddox, A.S., Lewellyn, L., Desai, A., and Oegema, K. (2007). Anillin and the septins promote asymmetric ingression of the cytokinetic furrow. Dev Cell *12*, 827-835.

Mathieu, J., Cauvin, C., Moch, C., Radford, S.J., Sampaio, P., Perdigoto, C.N., Schweisguth, F., Bardin, A.J., Sunkel, C.E., Mckim, K., *et al.* (2013). Aurora B and Cyclin B Have Opposite Effects on the Timing of Cytokinesis Abscission in Drosophila Germ Cells and in Vertebrate Somatic Cells. Dev Cell *26*, 250-265.

McLachlan, I.G., and Heiman, M.G. (2013). Shaping dendrites with machinery borrowed from epithelia. Curr Opin Neurobiol *23*, 1005-1010.

McLean, P.F., and Cooley, L. (2013). Protein Equilibration Through Somatic Ring Canals in Drosophila. Science *340*, 1445-1447.

Morais-de-Sa, E., and Sunkel, C. (2013). Adherens junctions determine the apical position of the midbody during follicular epithelial cell division. Embo Rep *14*, 696-703.

Nechipurenko, I.V., Berciu, C., Sengupta, P., and Nicastro, D. (2017). Centriolar remodeling underlies basal body maturation during ciliogenesis in Caenorhabditis elegans. eLife *6*.

Norden, C., Mendoza, M., Dobbelaere, J., Kotwaliwale, C.V., Biggins, S., and Barral, Y. (2006). The NoCut pathway links completion of cytokinesis to spindle midzone function to prevent chromosome breakage. Cell *125*, 85-98.

Oegema, K., and Hyman, A.A. (2006). Cell division. WormBook : the online review of C elegans biology, 1-40.

Ou, G., Stuurman, N., D'Ambrosio, M., and Vale, R.D. (2010). Polarized myosin produces unequal-size daughters during asymmetric cell division. Science *330*, 677-680.

Ou, G.S., Gentili, C., and Gonczy, P. (2014). Stereotyped distribution of midbody remnants in early C. elegans embryos requires cell death genes and is dispensable for development. Cell Res *24*, 251-253.

Padmanabhan, A., and Zaidel-Bar, R. (2017). Non-junctional E-Cadherin Clusters Regulate the Actomyosin Cortex in the C. elegans Zygote. Mech Develop *145*, S85-S85.

Paolini, A., Duchemin, A.L., Albadri, S., Patzel, E., Bornhorst, D., Avalos, P.G., Lemke, S., Machate, A., Brand, M., Sel, S., *et al.* (2015). Asymmetric inheritance of the apical domain and self-renewal of retinal ganglion cell progenitors depend on Anillin function. Development *142*, 832-839.

Perkins, L.A., Hedgecock, E.M., Thomson, J.N., and Culotti, J.G. (1986). Mutant Sensory Cilia in the Nematode Caenorhabditis-Elegans. Developmental Biology *117*, 456-487.

Pohl, C., and Bao, Z. (2010). Chiral forces organize left-right patterning in C. elegans by uncoupling midline and anteroposterior axis. Dev Cell *19*, 402-412.

Pollarolo, G., Schulz, J.G., Munck, S., and Dotti, C.G. (2011). Cytokinesis remnants define first neuronal asymmetry in vivo. Nat Neurosci *14*, 1525-1533.

Portereiko, M.F., Saam, J., and Mango, S.E. (2004). ZEN-4/MKLP1 is required to polarize the foregut epithelium. Curr Biol *14*, 932-941.

Rasmussen, J.P., Feldman, J.L., Reddy, S.S., and Priess, J.R. (2013). Cell Interactions and Patterned Intercalations Shape and Link Epithelial Tubes in C. elegans. Plos Genetics *9*.

Rasmussen, J.P., Reddy, S.S., and Priess, J.R. (2012). Laminin is required to orient epithelial polarity in the C. elegans pharynx. Development *139*, 2050-2060.

Reinsch, S., and Karsenti, E. (1994). Orientation of Spindle Axis and Distribution of Plasma-Membrane Proteins during Cell-Division in Polarized Mdckii Cells. J Cell Biol *126*, 1509-1526.

Salzmann, V., Chen, C., Chiang, C.Y., Tiyaboonchai, A., Mayer, M., and Yamashita, Y.M. (2014). Centrosome-dependent asymmetric inheritance of the midbody ring in Drosophila germline stem cell division. Mol Biol Cell *25*, 267-275.

Sato, K., Norris, A., Sato, M., and Grant, B.D. (2014). C. elegans as a model for membrane traffic. WormBook : the online review of C elegans biology, 1-47.

Schiel, J.A., Childs, C., and Prekeris, R. (2013). Endocytic transport and cytokinesis: from regulation of the cytoskeleton to midbody inheritance. Trends Cell Biol *23*, 319-327.

Schiel, J.A., Park, K., Morphew, M.K., Reid, E., Hoenger, A., and Prekeris, R. (2011). Endocytic membrane fusion and buckling-induced microtubule severing mediate cell abscission. J Cell Sci *124*, 1411-1424.

Schindelin, J., Arganda-Carreras, I., Frise, E., Kaynig, V., Longair, M., Pietzsch, T., Preibisch, S., Rueden, C., Saalfeld, S., Schmid, B., *et al.* (2012). Fiji: an open-source platform for biological-image analysis. Nat Methods *9*, 676-682.

Schluter, M.A., Pfarr, C.S., Pieczynski, J., Whiteman, E.L., Hurd, T.W., Fan, S.L., Liu, C.J., and Margolis, B. (2009). Trafficking of Crumbs3 during Cytokinesis Is Crucial for Lumen Formation. Mol Biol Cell *20*, 4652-4663.

Schumacher, J.M., Golden, A., and Donovan, P.J. (1998). AIR-2: An Aurora/Ipl1-related protein kinase associated with chromosomes and midbody microtubules is required for polar body extrusion and cytokinesis in Caenorhabditis elegans embryos. J Cell Biol *143*, 1635-1646.

Severson, A.F., Hamill, D.R., Carter, J.C., Schumacher, J., and Bowerman, B. (2000). The Aurora-related kinase AIR-2 recruits ZEN-4/CeMKLP1 to the mitotic spindle at metaphase and is required for cytokinesis. Curr Biol *10*, 1162-1171.

Siller, K.H., and Doe, C.Q. (2009). Spindle orientation during asymmetric cell division. Nat Cell Biol *11*, 365-374.

Singh, D., and Pohl, C. (2014). Coupling of Rotational Cortical Flow, Asymmetric Midbody Positioning, and Spindle Rotation Mediates Dorsoventral Axis Formation in C. elegans. Dev Cell *28*, 253-267.

Skop, A.R., Liu, H., Yates, J., 3rd, Meyer, B.J., and Heald, R. (2004). Dissection of the mammalian midbody proteome reveals conserved cytokinesis mechanisms. Science *305*, 61-66.

Smith, K.P., Kieserman, E.K., Wang, P.I., Basten, S.G., Giles, R.H., Marcotte, E.M., and Wallingford, J.B. (2011). A Role for Central Spindle Proteins in Cilia Structure and Function. Cytoskeleton *68*, 112-124.

Steigemann, P., Wurzenberger, C., Schmitz, M.H.A., Held, M., Guizetti, J., Maar, S., and Gerlich, D.W. (2009). Aurora B-Mediated Abscission Checkpoint Protects against Tetraploidization. Cell *136*, 473-484.

Sulston, J.E., Schierenberg, E., White, J.G., and Thomson, J.N. (1983). The embryonic cell lineage of the nematode Caenorhabditis elegans. Dev Biol *100*, 64-119.

Tong, Y.G., and Burglin, T.R. (2010). Conditions for dye-filling of sensory neurons in Caenorhabditis elegans. J Neurosci Meth *188*, 58-61.

van Furden, D., Johnson, K., Segbert, C., and Bossinger, O. (2004). The C-elegans ezrin-radixin-moesin protein ERM-1 is necessary for apical junction remodelling and tubulogenesis in the intestine. Developmental Biology *272*, 262-276.

Von Stetina, S.E., Liang, J., Marnellos, G., and Mango, S.E. (2017). Temporal regulation of epithelium formation mediated by FoxA, MKLP1, MgcRacGAP, and PAR-6. Mol Biol Cell *28*, 2042-2065.

Waddle, J.A., Cooper, J.A., and Waterston, R.H. (1994). Transient localized accumulation of actin in Caenorhabditis elegans blastomeres with oriented asymmetric divisions. Development *120*, 2317-2328.

Wang, J., Silva, M., Haas, L.A., Morsci, N.S., Nguyen, K.C.Q., Hall, D.H., and Barr, M.M. (2014a). C-elegans Ciliated Sensory Neurons Release Extracellular Vesicles that Function in Animal Communication. Curr Biol *24*, 519-525.

Wang, T., Yanger, K., Stanger, B.Z., Cassio, D., and Bi, E. (2014b). Cytokinesis defines a spatial landmark for hepatocyte polarization and apical lumen formation. Journal of Cell Science *127*, 2483-2492.

Wilcock, A.C., Swedlow, J.R., and Storey, K.G. (2007). Mitotic spindle orientation distinguishes stem cell and terminal modes of neuron production in the early spinal cord. Development *134*, 1943-1954.

Yang, R.Z., and Feldman, J.L. (2015). SPD-2/CEP192 and CDK Are Limiting for Microtubule-Organizing Center Function at the Centrosome. Curr Biol *25*, 1924-1931.

Zenker, J., White, M.D., Templin, R.M., Parton, R.G., Thorn-Seshold, O., Bissiere, S., and Plachta, N. (2017). A microtubule-organizing center directing intracellular transport in the early mouse embryo. Science *357*, 925-+.

Figure 1

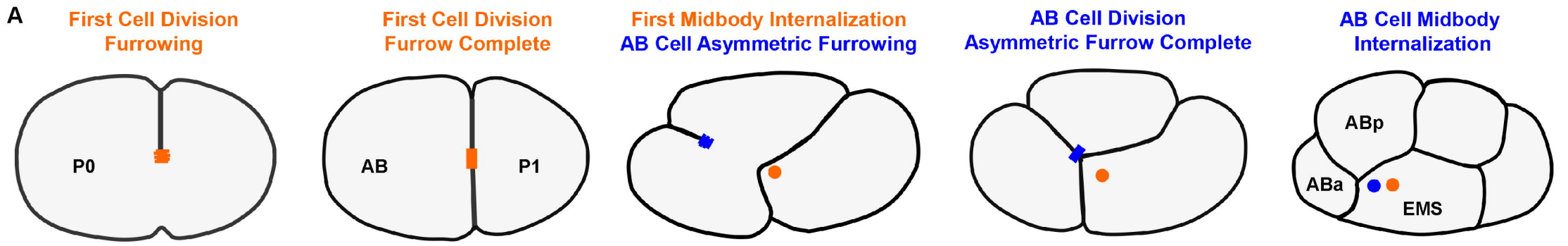

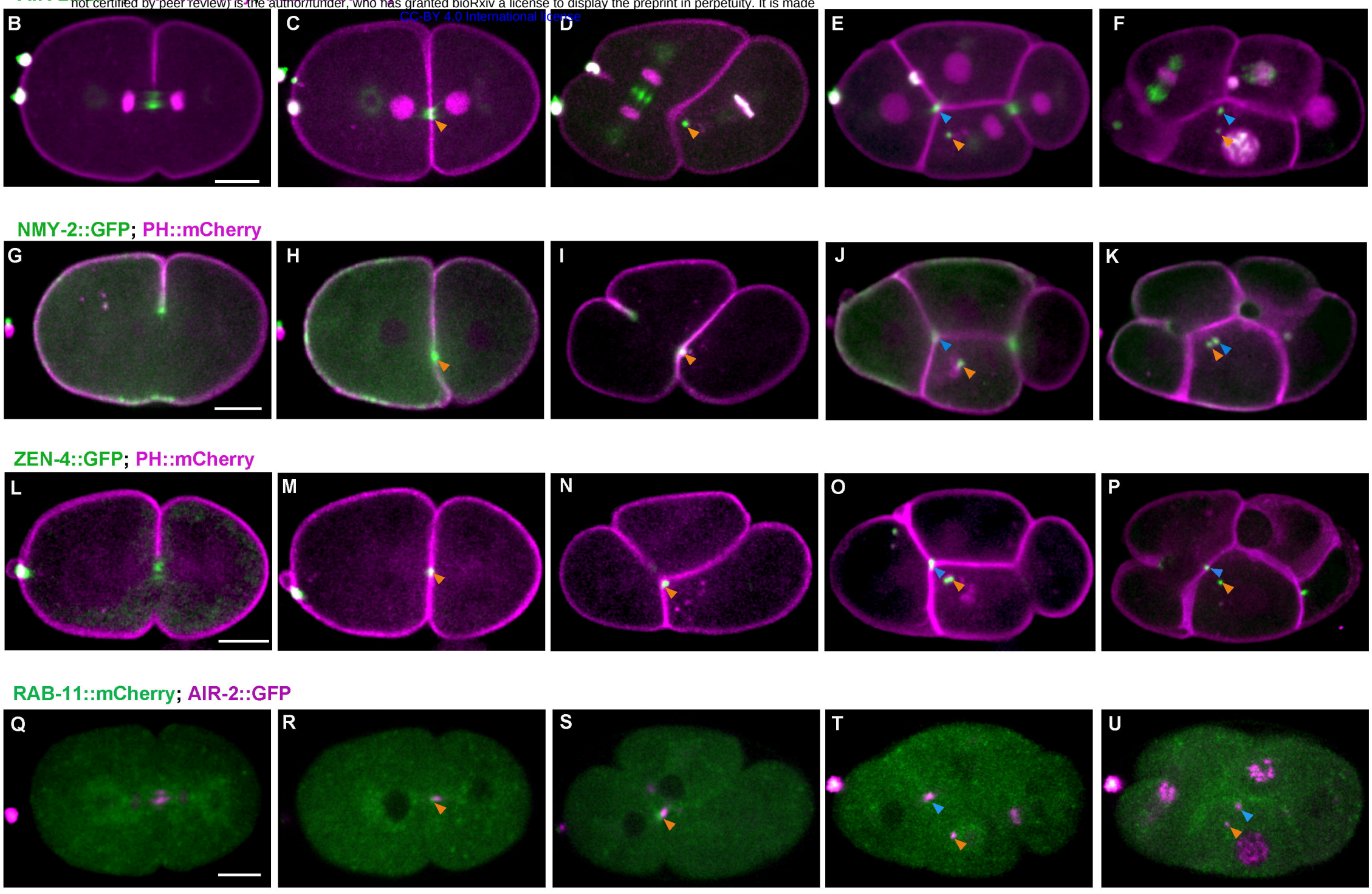

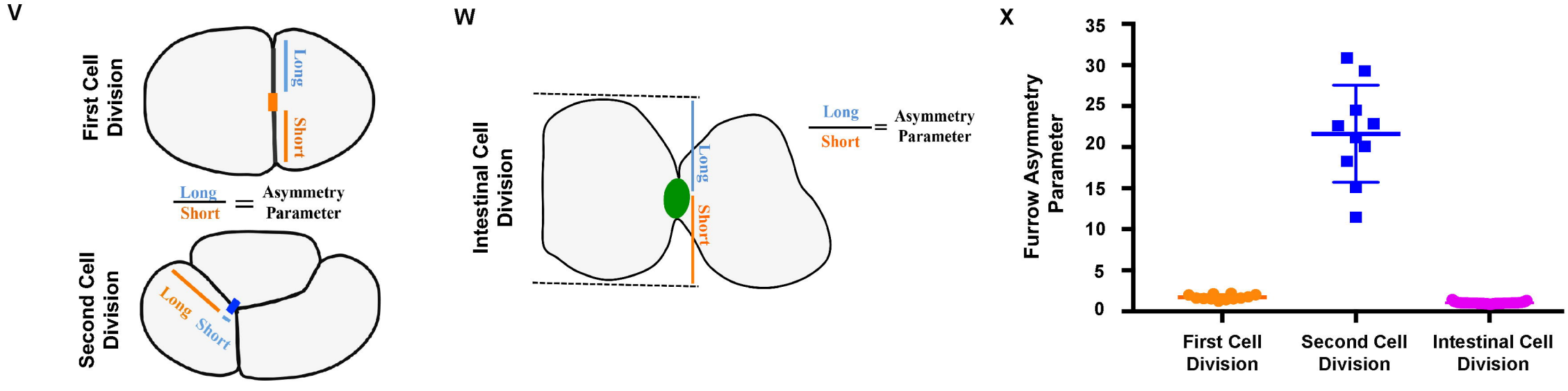

Figure 2

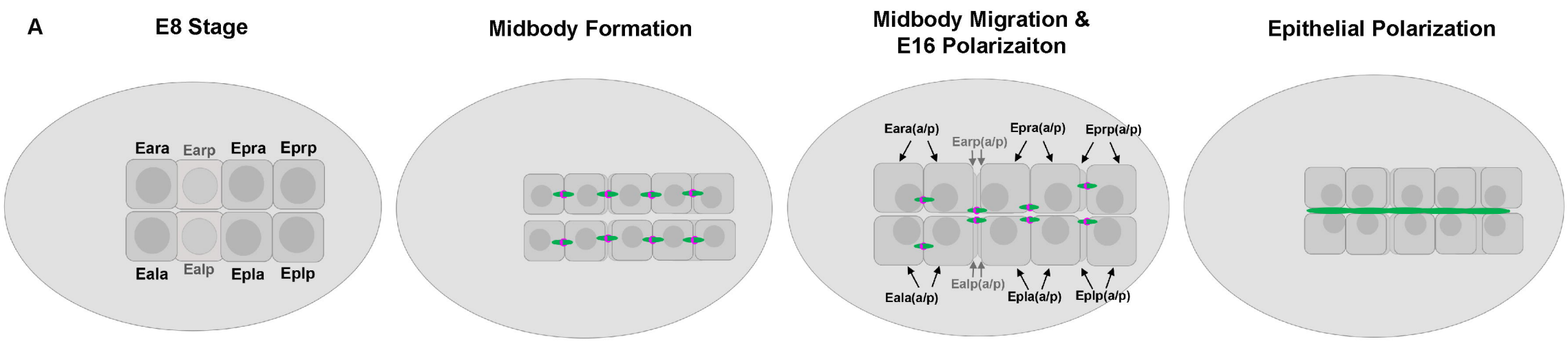

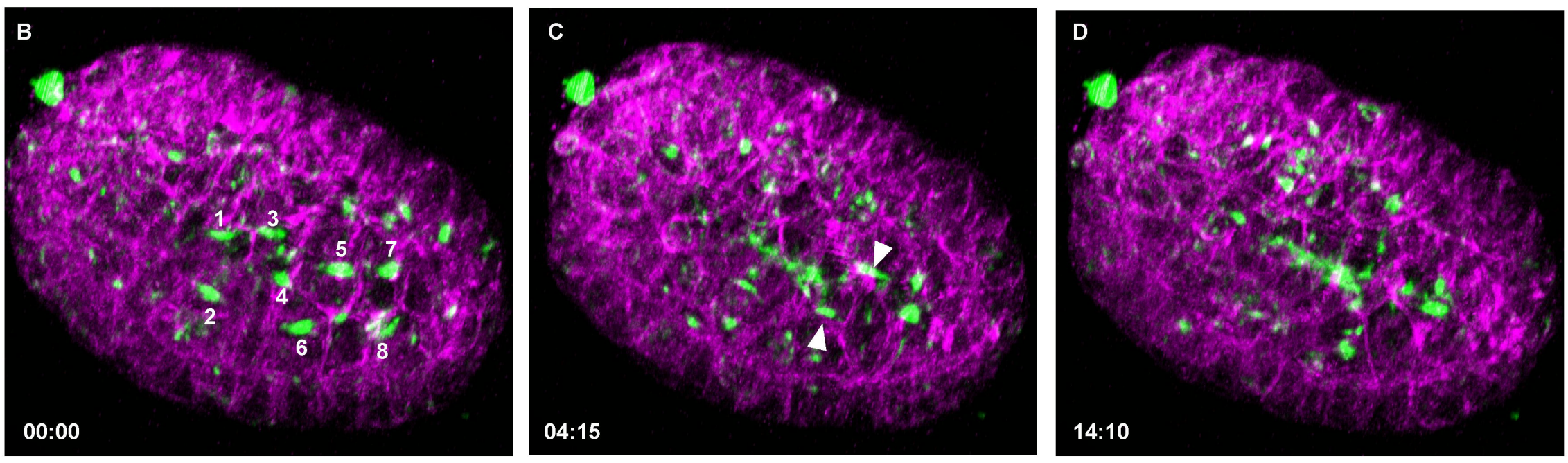

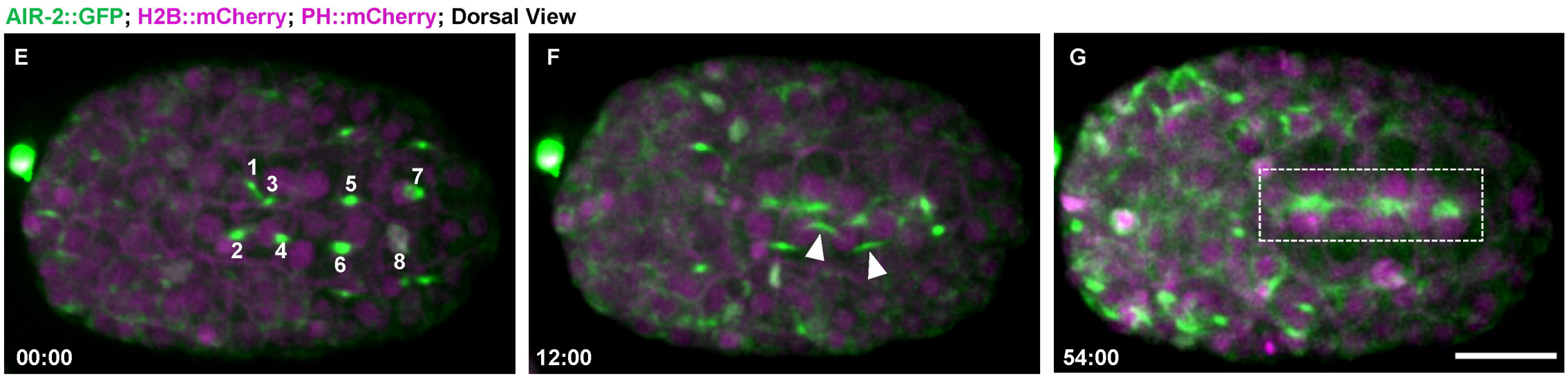

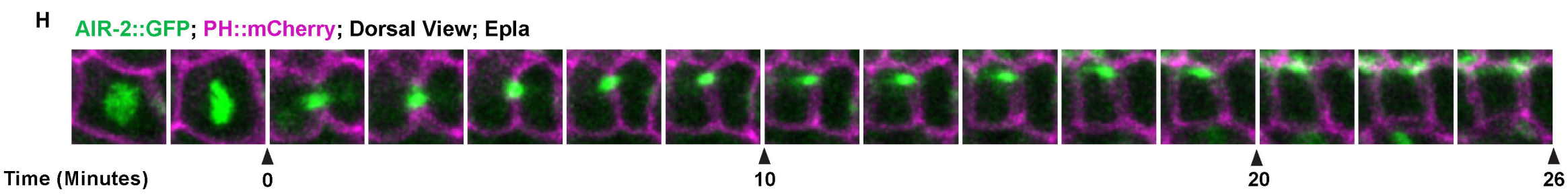

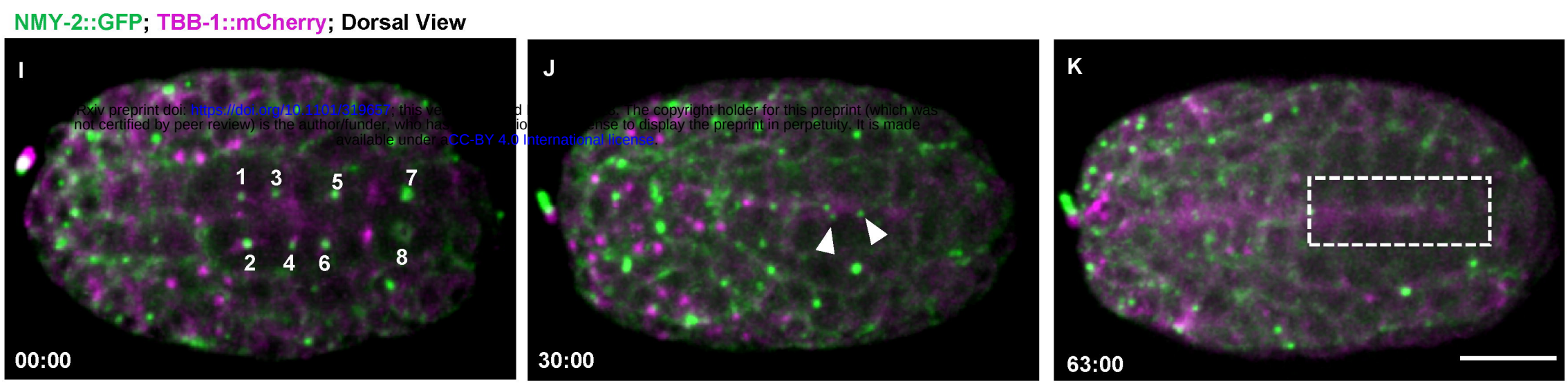

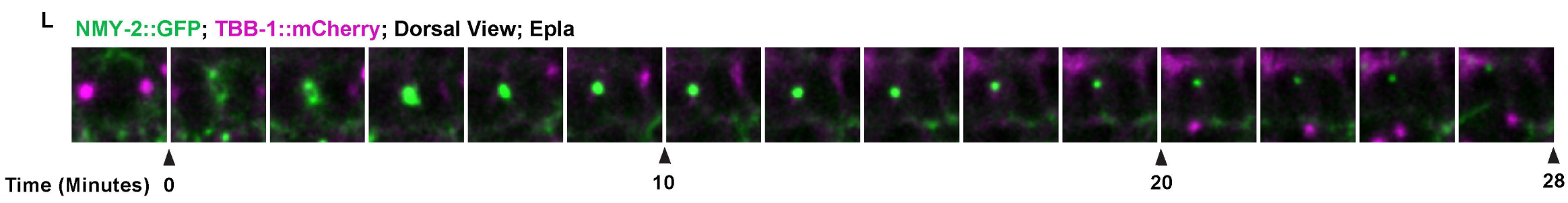

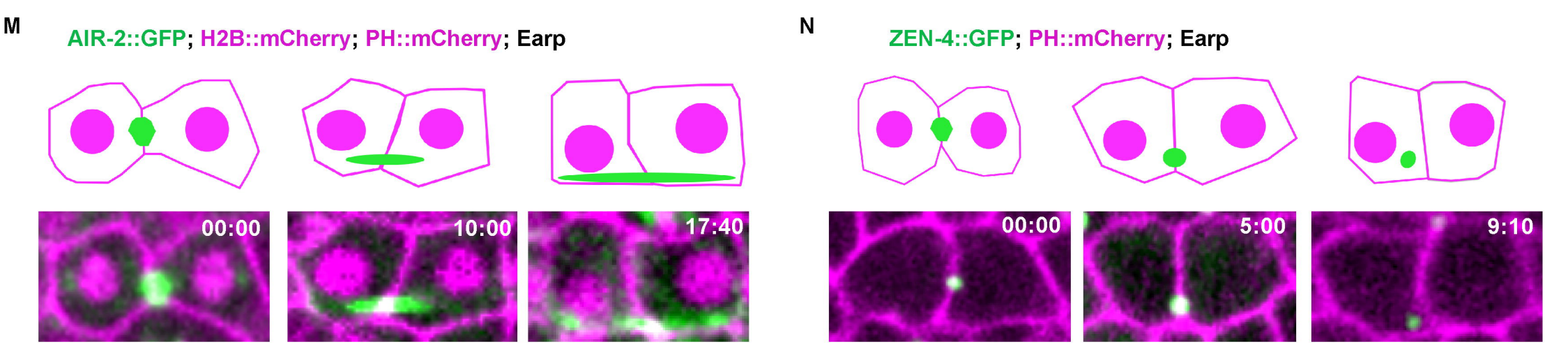

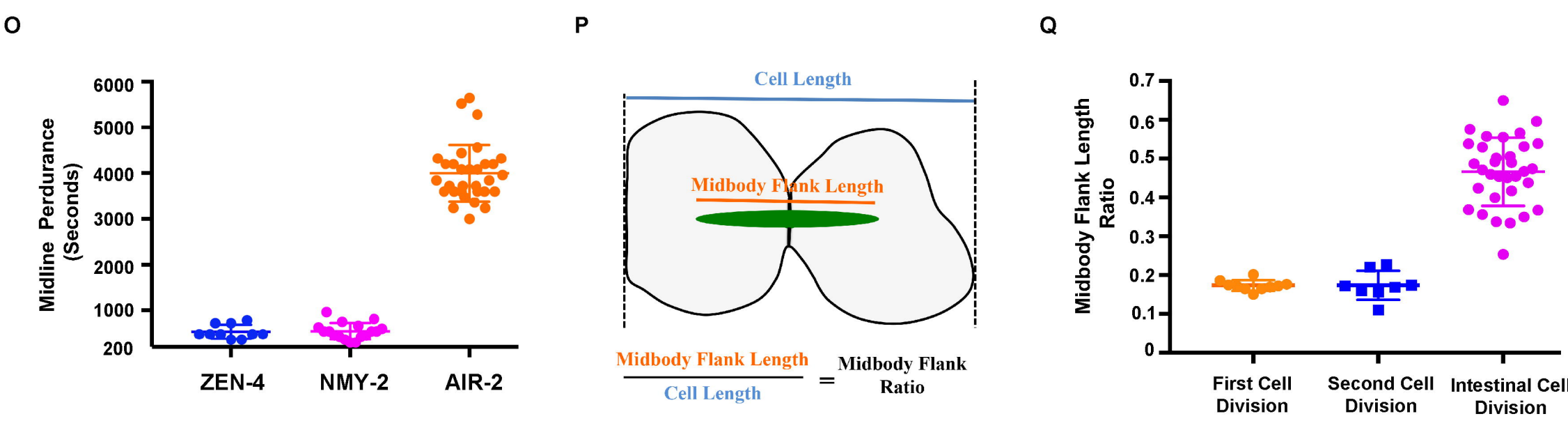

Figure 3

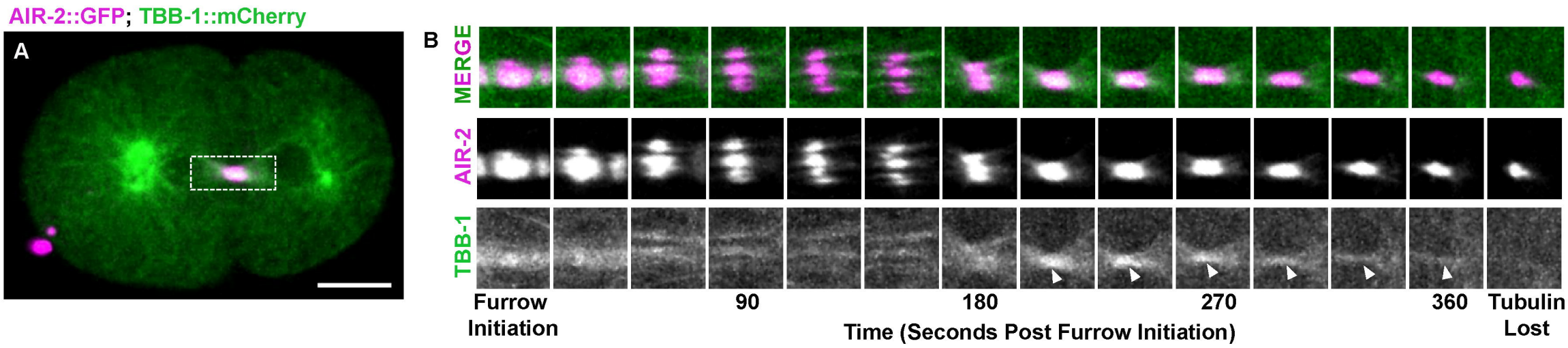

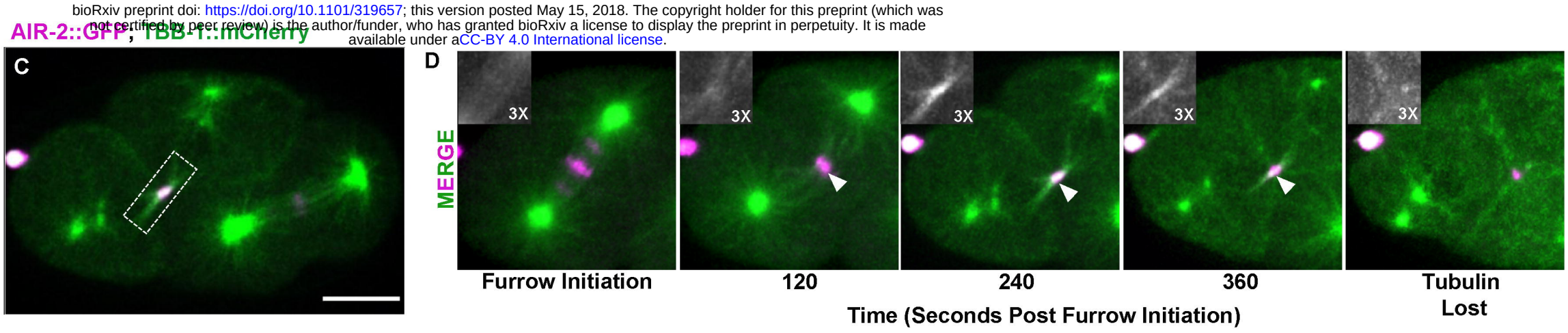

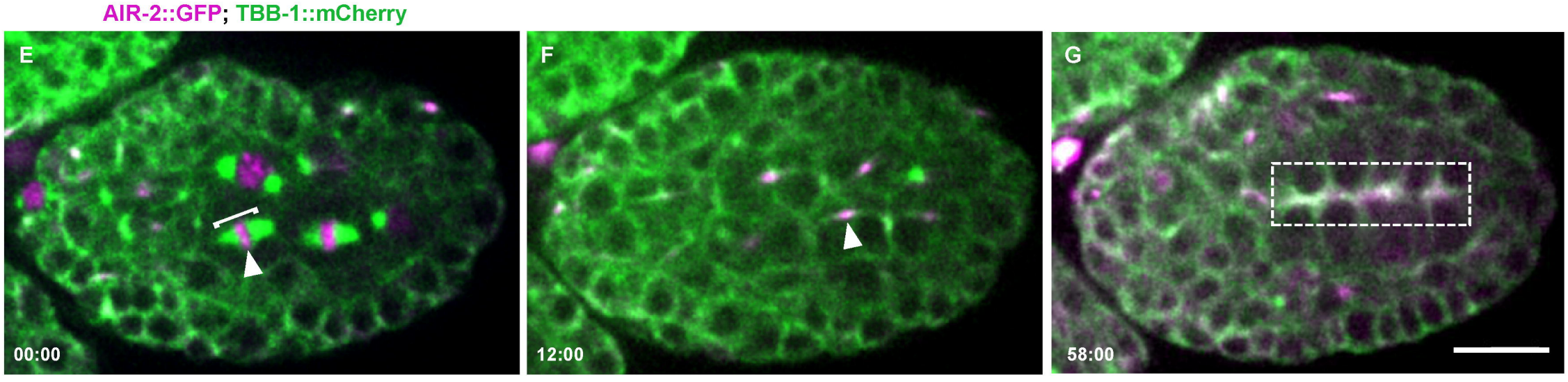

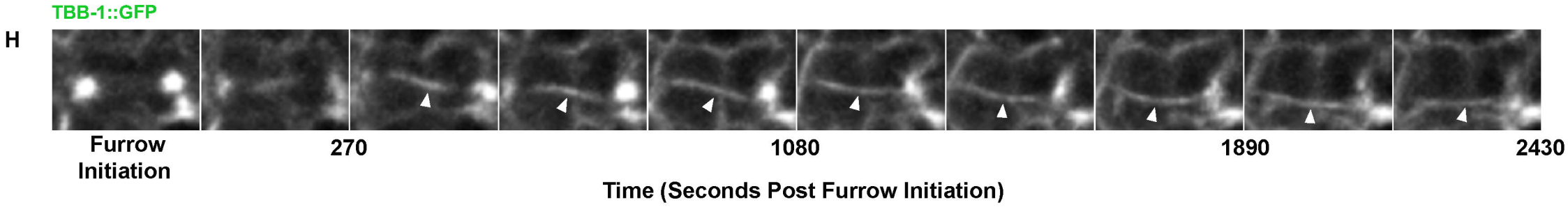

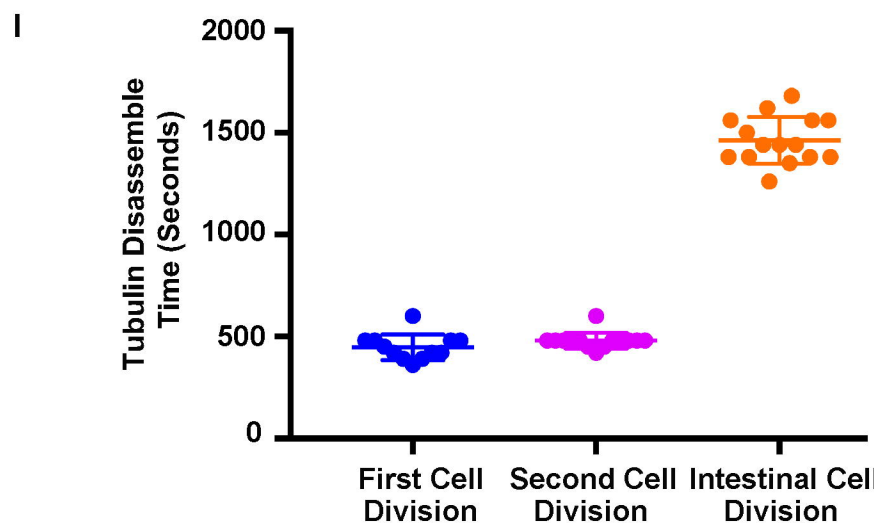

Figure 4

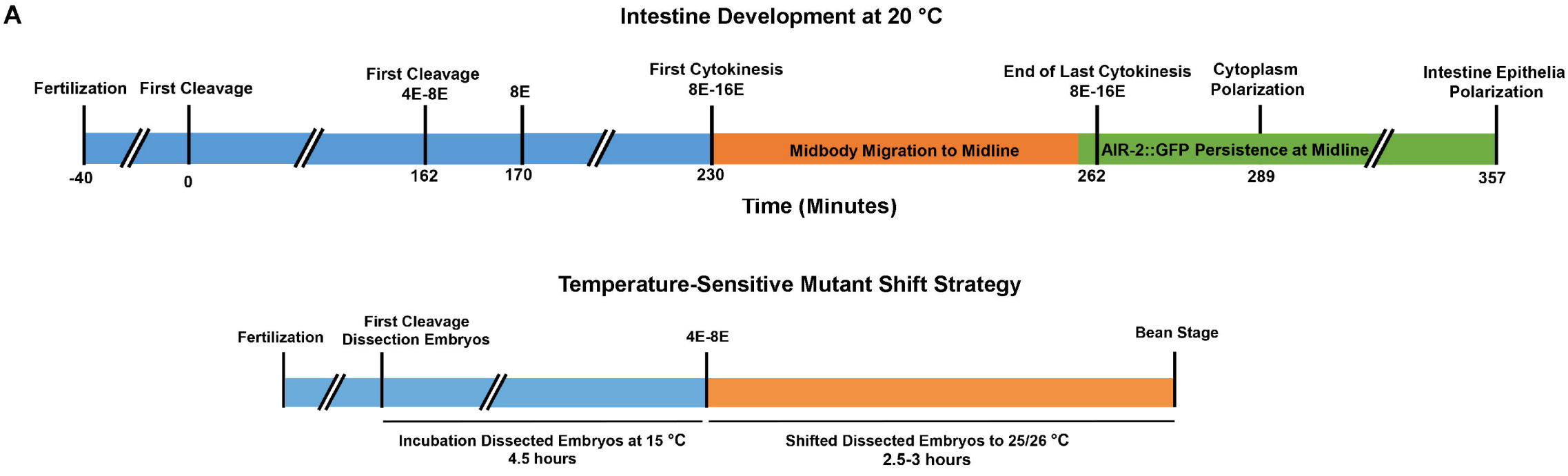

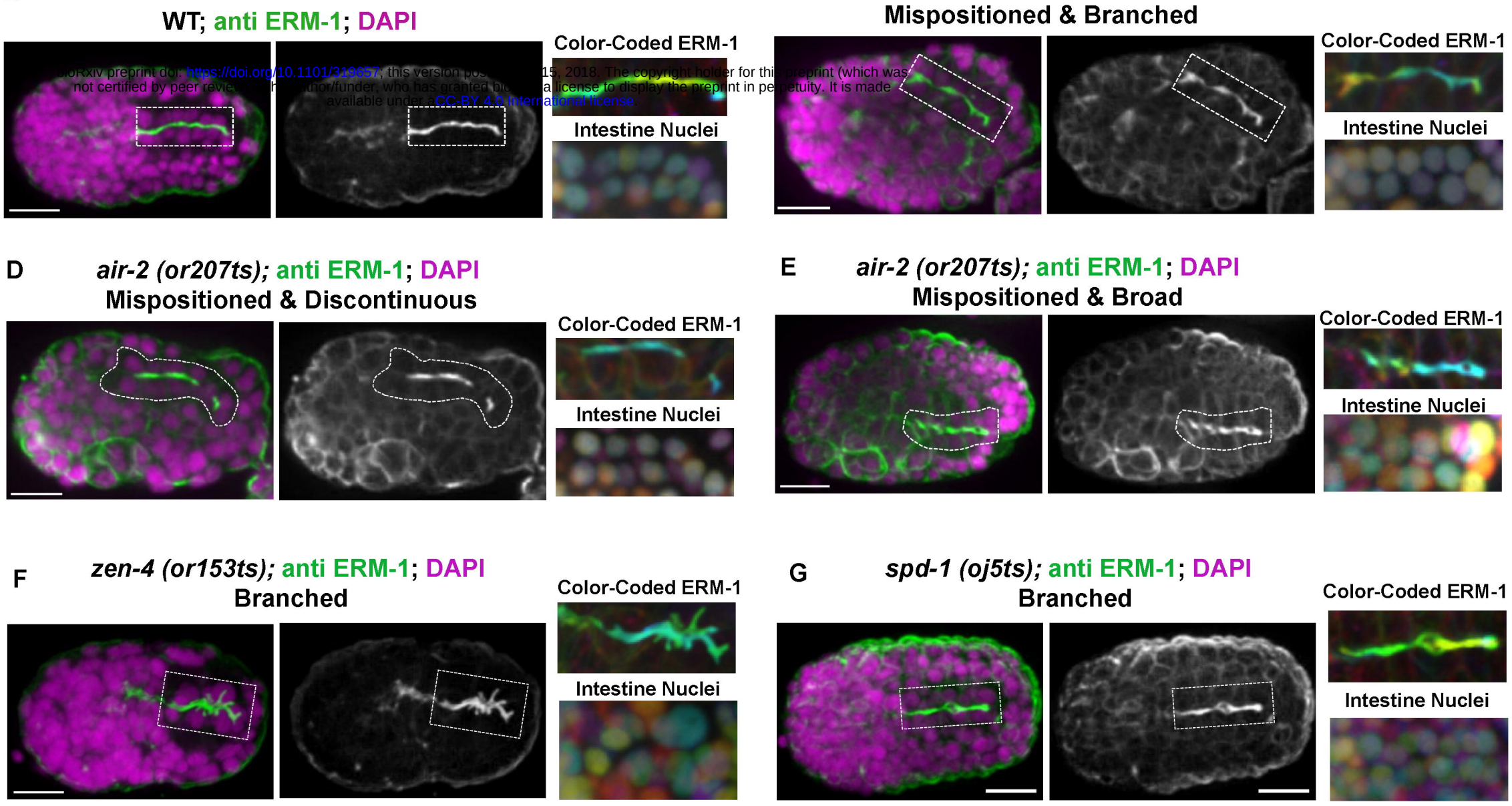

H

	Mispositioned	Discontinuous	Broad	Branched
WT (N2)	0% (0/60)	0% (0/60)	3.3% (2/60)	20% (12/60)
air-2 (or207ts)	60.9% (25/41)	43.9% (18/41)	12.1% (5/41)	65.9% (27/41)
zen-4 (or153ts)	27.3% (6/22)	27.3% (6/22)	81.8% (18/22)	81.8% (18/22)
spd-1 (oj5ts)	0% (0/59)	28.8% (17/59)	10.2% (6/59)	40% (24/59)

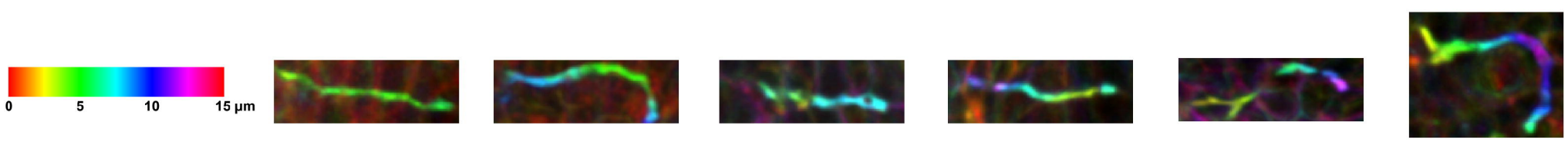

	One Color	Two Color	Three Color	Four Color	Five Color	Six Color
WT (N2)	25% (15/60)	40% (24/60)	31.7% (19/60)	3.3% (2/60)	0% (0/60)	0% (0/60)
air-2 (or207ts)	0% (0/41)	22.0% (9/41)	12.2% (9/41)	34.1% (14/41)	14.6% (6/41)	17.1% (7/41)
zen-4 (or153ts)	0% (0/22)	27.3% (6/22)	40.9% (9/22)	22.7% (5/22)	4.5% (1/22)	0% (0/22)
spd-1 (oj5ts)	10.2% (6/59)	55.9% (33/59)	27.1% (16/59)	1.7% (1/59)	1.7% (1/59)	0% (0/59)

Figure 5

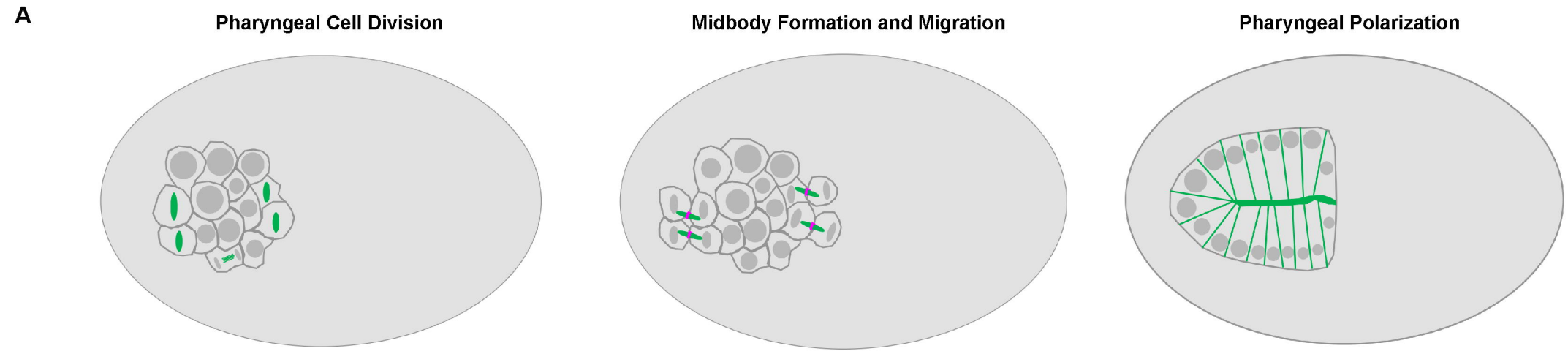

AIR-2::GFP; H2B::mCherry; Ventral View

Dorsal View after E16 Polarization

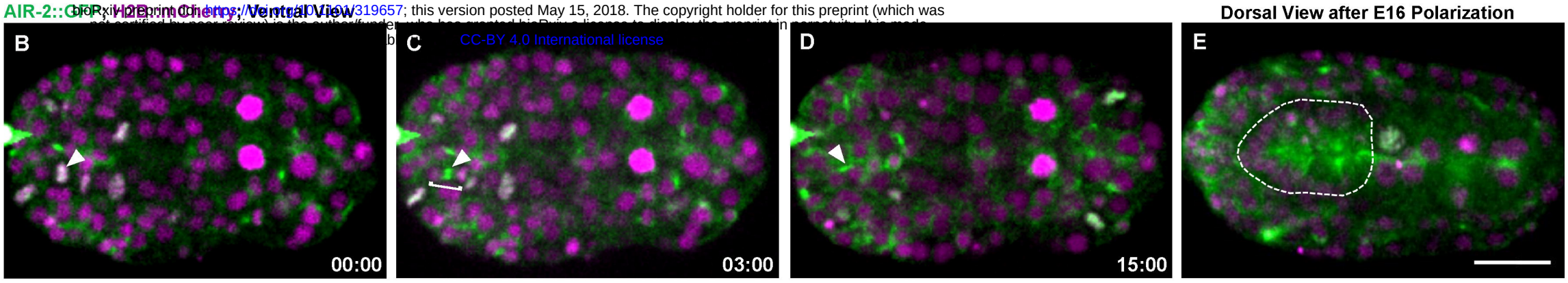

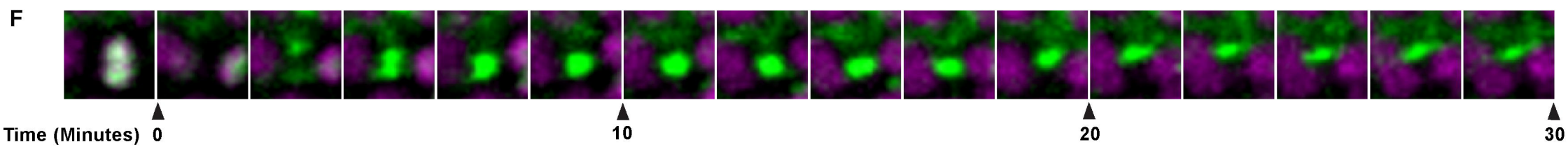

ZEN-4::GFP; TBB-1::mCherry; Ventral View

Dorsal View after E16 Polarization

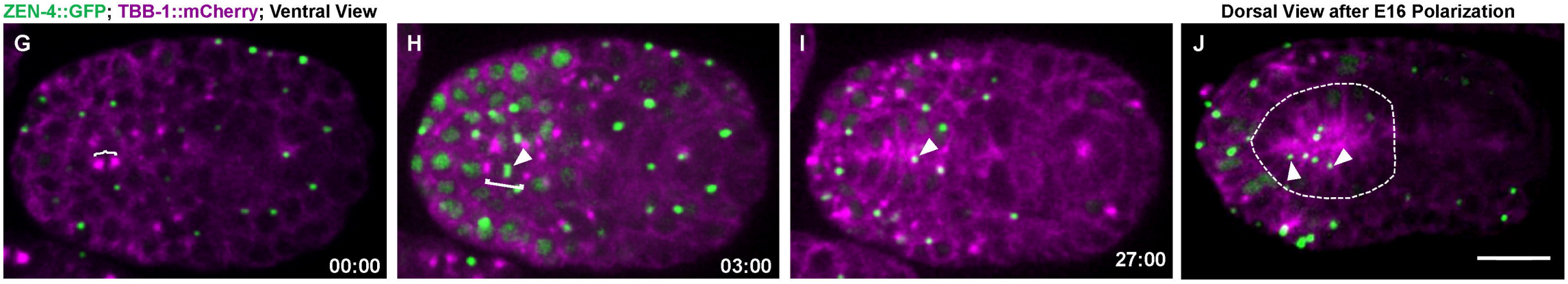

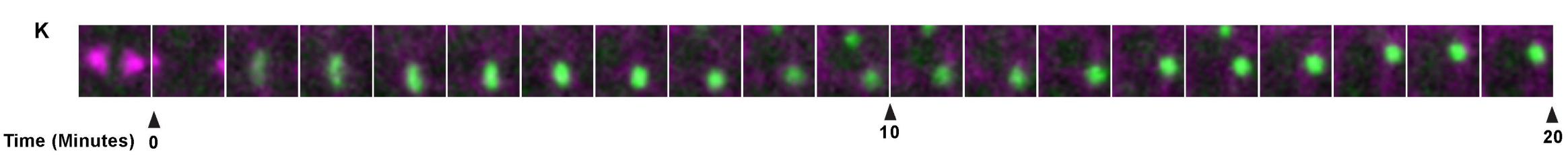

NMY-2::GFP; TBB-1::mCherry; Ventral View

Dorsal View after E16 Polarization

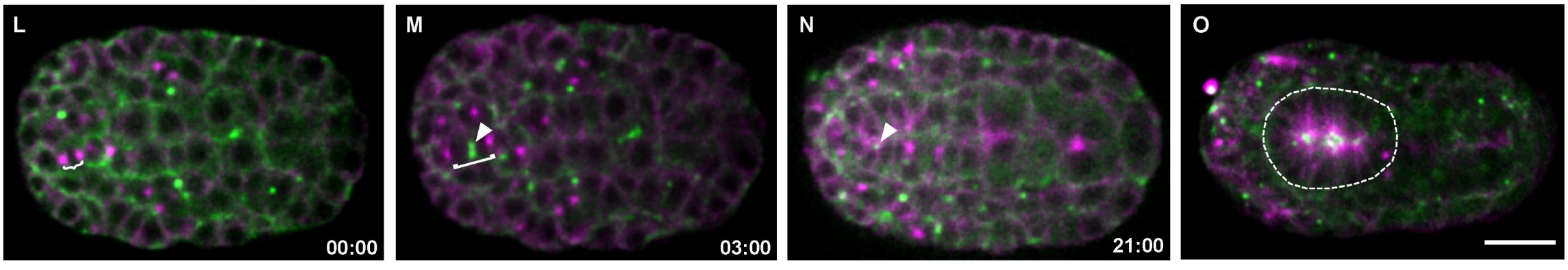

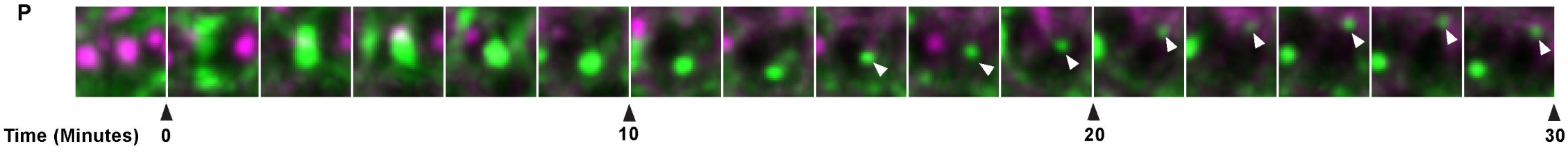

Figure 6

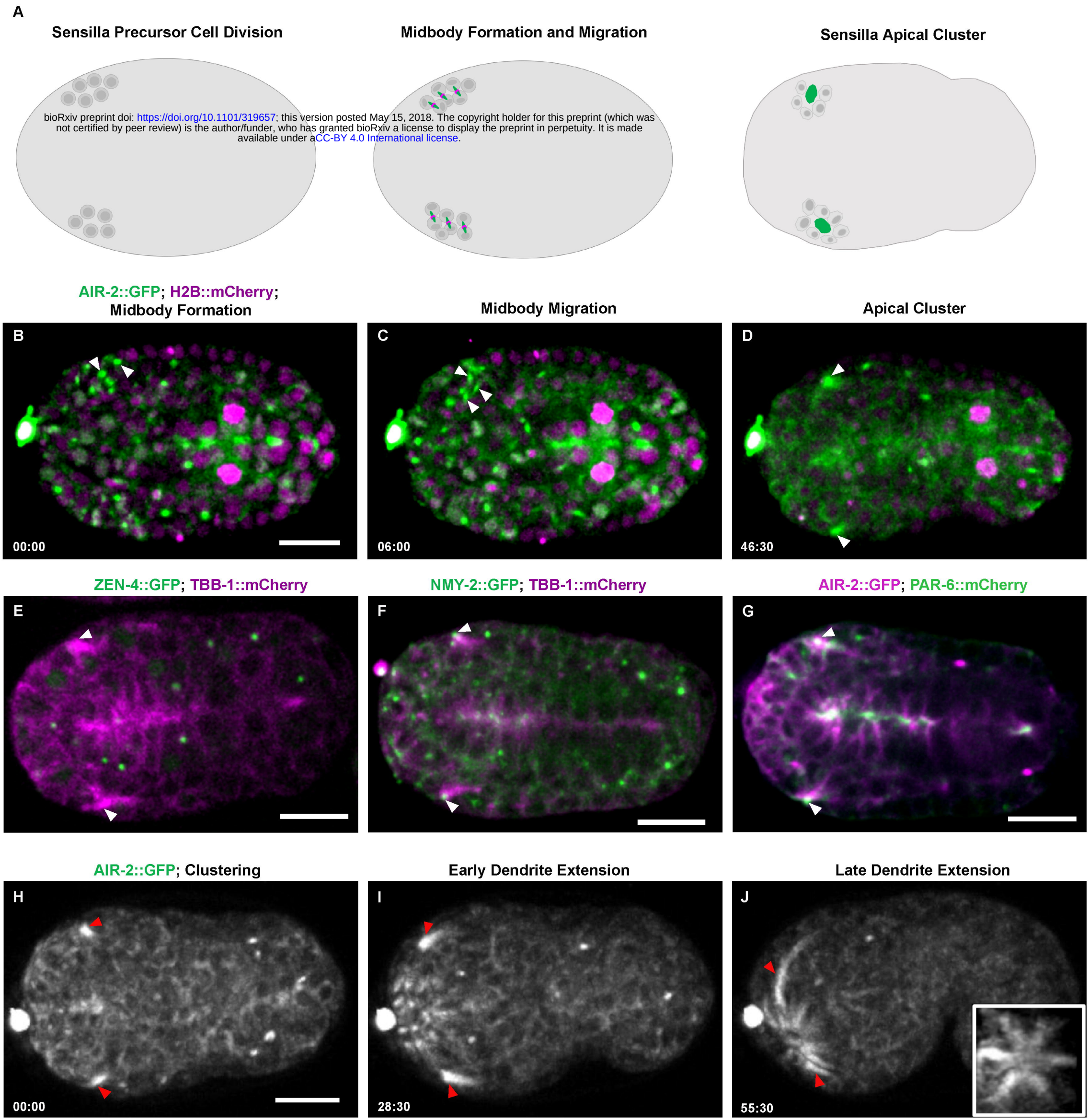

Figure 7